

Response to the Referee

Comments and responses:

General comments

5 The article presents a comparison among five machine-learning methods (k-nearest neighbor, multilayer neural network, random forest, support vector machines and extreme gradient boosting), when applied to the spatial analysis of soil particle-size fractions collected in the Heihe River Basin (China), together with environmental covariates (topographic, remote sensing, climate, soil physicochemical attributes and categorical maps). The performances of the methods are tested when data are considered both on the original scale, and on a log-ratio basis. In the latter case, the authors consider three transformations widely used in compositional data analysis, i.e., additive log-ratio, centered log-ratio, isometric log-ratio. The comparison among methods is quantitatively performed through a Monte-Carlo procedure (30 repetitions of subsampling) on the basis of objective performance indicators (AUC, AUPRC for classification, R^2 , RMSE, MAE, AD, STRESS for regression). In my opinion, the paper is overall clear and the methods used fairly detailed. The models and methods chosen are overall appropriate.

10 **Response:** We thank the Anonymous Referee #1 for constructive comments, suggestions and encouragement. The positive comments have provided us encouragement to revise the paper to the best of our ability.

15 **However, it is not always explained how the methods were applied to the soil fraction vectors, i.e., whether they were applied jointly to the fractions or component-wise. This indeed makes a relevant difference, the former being definitely more meaningful than the latter.**

20 **Response:** For spatial prediction of soil particle size fractions as compositional data, models based on joint fractions such as Dirichlet regression (Hijazi and Jernigan, 2009) and compositional kriging combined with log ratio transformed data (Wang and Shi, 2017) can deliver stable performance. Additionally, independent models of component-wise using appropriate transformation methods and ancillary data were also widely applied for prediction. In our study, all machine-learning models using transformed data for prediction of soil psf were applied component-wise to the fractions, then the results were compared and evaluated on the original scale using inverse transformation equations.

25 **In general, I found interesting the thorough comparison of those machine learning methods that are nowadays widely used, and particularly the comparison of the two views of the Euclidean and the Compositional geometry. However, I have two main concerns – reported in the next section – on the approach used by the authors for the investigation, related with two points that, in my view, would be relevant for the topic of the paper but are not considered by the authors.**

Specific comments

Comment 1: Uncertainty

The authors do not address the key topic of uncertainty, neither in the results of classification/regression, nor in the performance indicators. In fact, it would be key to understand the degree of uncertainty associated with the results, and if the used method can indeed provide a clear indication of the variability of the estimates and not only the estimates themselves. In a Monte Carlo study, one should also verify (i) if the estimators' variability has a reasonable order of magnitude with respect to the values of the estimates and (ii) if it is representative of the actual error that one makes on an independent test set. In fact, the results provided by different methods and compared in the paper may be even indistinguishable if their variability is high. I do believe that point estimates are relevant, but their uncertainty does provide a meaningful information that in my view cannot left out of this kind of comparisons. In addition, the authors should indicate the standard deviation of the indicators of performance (e.g., those in Table 2), to appreciate the stability of the results across the repetitions with different sampling points.

Response: Thanks for the referee's suggestions about the uncertainty assessment of our research, and we agree that it is very important for spatial prediction to describe the stability and variability of different models and methods not only in regression of soil psf but also in classification of soil texture. For interpolation of soil psf, the standard deviation (SD) and the ranges of 95 % confidence interval (CI) of the indicators were calculated in our revised manuscript. For soil texture classification, confusion index (COI) was calculated on each independent test to describe the uncertainty of each machine-learning method, which delivered different confusion of model.

(Page 23, L10-L15) *"The accuracy and performance of machine-learning models mentioned above for the original (untransformed) and different log ratio transformation approaches were evaluated using five statistical indicators, containing coefficient of determination (R^2), root mean square error (RMSE), mean absolute error (MAE), Aitchison distance (AD) (Aitchison, 1992), and standardized residual sum of squares (STRESS) (Martin-Fernandez et al., 2001). For the assessment of model uncertainty, the standard deviation (SD) and the ranges of 95 % confidence interval (CI) (Streiner, 1996) of indicators derived from running models 30 times were generated as indicators of prediction uncertainties."*

(Page 32, L25-L32 and Page 32, L1-L3) *"For the assessments of the uncertainties of models, we calculated the standard deviation (SD) of prediction values, Table 4 showed that all machine-learning models produced low SDs of these indicators, revealing stable performance. Additionally, ORI approach delivered lower SDs than those of log ratio approaches among five machine-learning models for sand, silt and clay. For the comparison of SD of three log ratio approaches, they generated almost the same results. Moreover, the ranges of 95 % confidence interval (CI) of indicators were also computed (Table 5), which indicated relatively low values compared with assessment indicators. For KNN, MLP and RF, the ORI approach showed lower values of CI of RMSE, MAE and R^2 than those of log ratio approaches, and for SVM and XGB, SVM_CLR*

and XGB_CLR revealed slight better performance compared with ORI for sand (CI_RMSE: 0.49 %; CI_MAE: 0.33 %) and silt (CI_MAE: 0.44 %), respectively. For the values of the ranges of 95 % CI of AD and STRESS, all models generated the same results (AD: 0.03, STRESS: 0.01) aside from RF_ILR (AD: 0.02), showing better performance. Thus, the estimators' variabilities had reasonable order of magnitudes for the values of the estimates and these indicators were representative of the actual errors on independent test sets."

5 (Pages 34-35, Table 4 and Table 5)

	SD			RMSE (%)			MAE (%)			R ² (%)			AD	STRESS
	Sand	Silt	Clay	Sand	Silt	Clay	Sand	Silt	Clay	Sand	Silt	Clay		
KNN_ALR	0.18	0.14	0.08	16.05	15.04	7.12	11.35	10.93	5.59	47.02	36.11	41.07	0.90	0.62
KNN_CLR	0.18	0.14	0.08	15.82	14.77	7.09	11.21	10.74	5.58	48.48	38.37	41.43	0.88	0.62
KNN_ILR	0.18	0.14	0.08	15.82	14.82	7.14	11.22	10.84	5.60	48.46	37.88	40.74	0.88	0.64
KNN_ORI	0.15	0.11	0.07	15.51	14.47	7.05	11.12	10.51	5.49	50.59	40.92	42.24	0.84	0.66
MLP_ALR	0.17	0.13	0.06	15.83	15.07	7.43	11.42	11.06	5.97	48.50	35.82	35.79	0.92	0.66
MLP_CLR	0.16	0.13	0.06	15.84	15.07	7.41	11.45	11.05	5.96	48.42	35.86	36.19	0.92	0.66
MLP_ILR	0.16	0.13	0.06	15.84	15.07	7.40	11.46	11.04	5.95	48.40	35.85	36.32	0.92	0.66
MLP_ORI	0.15	0.11	0.06	15.80	14.72	6.96	11.50	10.85	5.52	48.75	38.84	43.72	0.90	0.68
RF_ALR	0.18	0.15	0.08	15.50	14.43	6.62	10.90	10.52	5.24	50.57	41.23	48.90	0.86	0.61
RF_CLR	0.18	0.15	0.07	15.28	14.22	6.61	10.70	10.25	5.21	51.95	42.89	49.16	0.86	0.61
RF_ILR	0.18	0.15	0.08	15.27	14.25	6.66	10.66	10.26	5.26	51.99	42.60	48.28	0.86	0.61
RF_ORI	0.15	0.12	0.07	15.09	13.86	6.31	10.65	9.99	5.00	53.28	45.77	53.75	0.84	0.66
SVM_ALR	0.17	0.12	0.06	15.66	14.59	6.76	11.66	10.88	5.34	49.61	39.87	46.89	0.88	0.66
SVM_CLR	0.16	0.12	0.06	15.27	14.36	6.87	11.01	10.41	5.41	52.12	41.85	45.14	0.87	0.65
SVM_ILR	0.16	0.12	0.06	15.29	14.37	6.84	10.92	10.43	5.42	51.99	41.69	45.58	0.87	0.65
SVM_ORI	0.15	0.11	0.06	15.30	14.38	6.92	10.94	10.32	5.43	51.98	41.71	44.45	0.87	0.67
XGB_ALR	0.17	0.14	0.07	15.82	14.92	6.72	11.32	11.01	5.35	48.57	37.23	47.44	0.88	0.64
XGB_CLR	0.19	0.15	0.07	15.70	14.80	6.75	10.96	10.67	5.39	49.23	38.10	46.90	0.88	0.62
XGB_ILR	0.17	0.13	0.08	15.45	14.57	6.75	10.91	10.52	5.36	50.88	40.01	47.01	0.88	0.63
XGB_ORI	0.16	0.12	0.06	15.15	14.05	6.47	10.88	10.15	5.15	52.85	44.27	51.36	0.86	0.68

	CI_RMSE (%)			CI_MAE (%)			CI_R ² (%)			CI_AD	CI_STRESS
	Sand	Silt	Clay	Sand	Silt	Clay	Sand	Silt	Clay		
KNN_ALR	0.71	0.65	0.25	0.51	0.44	0.16	4.45	5.03	4.18	0.03	0.01
KNN_CLR	0.71	0.64	0.26	0.47	0.41	0.16	4.57	4.95	4.23	0.03	0.01
KNN_ILR	0.73	0.64	0.27	0.48	0.41	0.16	4.78	5.18	4.40	0.03	0.01
KNN_ORI	0.55	0.51	0.28	0.38	0.37	0.19	3.41	3.48	4.00	0.03	0.01
MLP_ALR	0.65	0.67	0.33	0.38	0.41	0.20	4.21	5.07	5.44	0.03	0.01
MLP_CLR	0.64	0.65	0.32	0.38	0.41	0.19	4.07	4.96	5.12	0.03	0.01
MLP_ILR	0.64	0.65	0.32	0.37	0.41	0.20	4.04	4.95	5.04	0.03	0.01
MLP_ORI	0.65	0.58	0.23	0.37	0.40	0.17	3.72	4.02	2.72	0.31	0.23
RF_ALR	0.62	0.54	0.25	0.42	0.38	0.17	4.03	3.91	4.03	0.03	0.01
RF_CLR	0.66	0.64	0.27	0.42	0.42	0.18	4.25	4.45	4.12	0.03	0.01
RF_ILR	0.69	0.66	0.27	0.44	0.42	0.18	4.34	4.75	4.31	0.02	0.01
RF_ORI	0.53	0.54	0.25	0.40	0.41	0.16	2.95	3.47	3.06	0.03	0.01
SVM_ALR	0.45	0.49	0.25	0.35	0.43	0.17	3.27	3.74	2.82	0.03	0.01
SVM_CLR	0.49	0.50	0.27	0.33	0.35	0.18	3.05	3.35	3.47	0.03	0.01
SVM_ILR	0.51	0.51	0.25	0.34	0.36	0.18	3.07	3.38	3.18	0.03	0.01
SVM_ORI	0.51	0.49	0.25	0.34	0.35	0.17	2.92	3.14	2.95	0.03	0.01
XGB_ALR	0.67	0.57	0.23	0.48	0.41	0.16	4.07	3.97	3.60	0.03	0.01
XGB_CLR	0.73	0.65	0.25	0.44	0.44	0.16	4.90	5.00	3.82	0.03	0.01
XGB_ILR	0.72	0.69	0.26	0.46	0.48	0.19	4.52	4.86	4.44	0.03	0.01
XGB_ORI	0.60	0.61	0.24	0.41	0.46	0.16	3.40	4.03	2.90	0.03	0.01

(Page 22, L28-L31 and Page 23, L1-L2) “Similarly, confusion index (COI) based on prediction probability was calculated to evaluate the uncertainties of machine-learning models of classification (Burrough et al., 1997), which equation was as follows:

$$COI = [1 - (P_{max,i} - P_{secmax,i})], \quad (1)$$

where $P_{max,i}$ refers to the maximum value of probability at position i and $P_{secmax,i}$ represents the second highest value of probability at position i , the lower COI, the better performance of model.”

(Page 27, L11-L13) “With respect to the uncertainties of models with confusion indices (COIs), RF (0.49) delivered the best performance, followed by KNN (0.50), SVM (0.54) and MLP (0.55); XGB (0.72) demonstrated the highest confusion of models (Table 3).”

(Page 29, Table 3)

	KNN	MLP	RF	SVM	XGB
COI	0.50	0.55	0.49	0.54	0.72

Comment 2: Generality of the results

The work provides a very broad comparison among the (classification or prediction) results obtained with different methods. However, it is not clear to me how general these results indeed are and thus how usable they will be for other scientists, that more likely work in other context than the field study here considered. In fact, even if I see the value of the Monte Carlo study and the quantitative indices it provides, I'm less convinced on the evaluation of the methods in terms of classification and prediction power for regions where no data is available (section 3.2.2, 3.3.2) – i.e., where it is hard to say which result is actually better than the others. It would be much easier (and convincing) to evaluate the method performances on a large scale simulated case rather than on this field case, at least for what concerns the classification and prediction in areas far from the data – and this would also provide a more general indications to other scientists.

Response: Thanks for the referee's suggestion about the general validity of our work. We quite agree with the referee's opinion that comparison (or evaluation) of the region where there is no data is unconvincing; even more detailed information is produced; it is hard to argue that this approach is better than others. In the revised manuscript, we focused on objectively revealing these results generated from different methods, including the indicators of abundance indices in classification, the value ranges of prediction maps, distribution characteristics and textural features, rather than subjectively describing which method is better than the others. With regard to your advice about the simulated case, it is the right direction, making evaluation more completed. However, soil particle size fractions we generated randomly were not according to the actual distribution such as the mutation values at adjacent positions. Moreover, the environmental covariates were hard to set well due to the variety. Therefore, it is hard to compare different machine-learning methods using environmental covariates and to produce more credible results of soil psf prediction by simulated case. However, we should pay more attention to it in our future research.

Technical corrections

Comment 1: If I understood correctly, the authors widely use the term “interpolation” to refer to the fit of the models. However, I'm not sure that all the models used are indeed interpolating the data.

Response: Thanks for the referee's question about “interpolation”. “Interpolation techniques” usually refer to the geostatistical analysis such as kriging methods, it also can be used to refer to the model fitting of machine-learning methods (see Buchanan et al., 2012; Deng et al., 2018; Niang et al., 2014). “Interpolation” was applied for the model of soil particle size fractions (continuous variables); however, there were no equations after fitting machine-learning models due to the nonlinearity of them.

Comment 2: P. 9 line 10: The fact that one variable would be omitted without loss of information does not provide a convincing explanation of why the Euclidean geometry is not appropriate to treat compositional data. I suggest to better explain the point.

Response: Thanks for the referee’s suggestion about a better explanation on why the Euclidean geometry is not appropriate to treat compositional data. In the revised version of **Page 19, L8-L16**, we paid more attention to explain the reason why the Euclidean geometry is not appropriate to deal with compositional data directly.

5 *“As compositional data, it is not common for soil particle size fractions (i.e. sand, silt and clay) to follow normal distribution (Lark and Bishop, 2007); moreover, because of the spurious correlations between components, different consequences would occur on different measurement scales, which makes more complicated interpretation (Abdi et al., 2015; Reimann and Filzmoser, 2000). Some significant principles such as scale invariance, sub-compositional coherence and dominance of compositions (Aitchison, 1997) should be taken into account in the compositional analysis. Indicators and statistical methods defined in the Euclidean geometry or based on Euclidean distances could reveal misleading or biased consequence (Butler, 10 1979) such as mean, median, standard deviation, standard PCA, analysis of the (co)variance, etc.”*

Further, the log-ratio approach provides a geometrical structure to the space of compositions, but it is not formally correct to say that the approach consists of the transformations alr, ilr, clr. Instead, it is more correct to say that the transformations ilr and clr can be used to operate within the log-ratio approach by simply using the Euclidean geometry on the transformed data.

15 **Response:** Thanks for the referee’s suggestion. We have modified the description of the relationship between log ratio approach and three transformation methods in the revised version in **Page 19, L16-L20**:

20 *“The most widely used approaches were so-called log ratio transformation (Aitchison, 1982), and the additive log ratio, centered log ratio and isometric log ratio (ALR, CLR, and ILR for short, respectively) from Aitchison (1982) and Egozcue et al. (2003) can be used to operate within the log-ratio approaches by simply using the Euclidean geometry on the transformed data.”*

One should also note that for a number of method (among which averaging and regression) ilr and clr provide equivalent results, whereas alr may provide different results.

25 **Response:** Thanks for the referee’s question about the relationship between ILR and CLR approaches. We have explained why **ilr and clr provide equivalent results in the revised manuscript in Page 44, L4-L11**.

30 *“Note that ILR and CLR approaches provided approximate equivalent consequences; firstly, ILR and CLR were isometric transformation methods, which could preserve distances; ALR however was not isometric. Secondly, CLR can transform into ILR using $(D - 1) \times D$ orthogonal identity matrix (Egozcue et al. 2003), ILR and CLR are the keys of the application of correlation analysis and principal component analysis (PCA) to compositions, respectively, and ILR variables should interpret and analyze in the CLR space in some cases (Grunsky, 2010). Further, slightly better performance of ILR than CLR were demonstrated in Table 4 because ILR overcomes the data collinearity problem and sub-compositional incoherence of CLR, by using an appropriate choice of the basis with regard to the latter case (Egozcue and Pawlowsky-Glahn, 2005).”*

Comment 3: P. 9 last line: it is not true that CLR is inapplicable – in fact, it is widely used in multivariate analyses.

Response: Thanks for the referee’s suggestion about CLR approach. We apologize for our mistake about this method description by using the word “inapplicable” to describe the shortcoming of CLR approach. We have corrected this statement in the revised version of **Page 20, L5-L7**.

“Nevertheless, the sum of the dimensions of CLR is 0, the problem of spurious correlation is still present (i.e. collinear).”

Comment 4: P. 10 line 2: It would be more appropriate to refer to Egozcue et al 2003.

Response: Thanks for the referee’s suggestion about reference citation and we have corrected this part in **Page 20, L9**.

“These problems can be overcome by using ILR, which transforms all the information into $D - 1$ orthogonal log contrasts (Egozcue et al. 2003).”

Comment 5: P. 10 line 15: the back-transformations are well known, the author should also refer to classical references appeared before their recent work.

Response: Thanks for the referee’s suggestion about reference citation and we have corrected this part by referring to the articles of Aitchison and Egozcue in the revised version of **Page 20, L21-L22**.

“The inverse transformation equations for ALR, CLR and ILR were recommended in their research (Aitchison, 1992; Egozcue et al., 2005).”

Comment 6: P. 12 line 15 and P. 16 line 15: if the ROC curve is not appropriate – as the author state – it should not be used for comparison.

Response: Thanks for the referee’s suggestion about the indicator of classification. We have deleted the ROC analysis of comparison of direct soil texture classification in the revised version.

Comment 7: P. 14 line 5 to 10: since the data are multivariate, multivariate notions of median (e.g., based on depth measures) should be used. Component-wise medians and quantiles should be avoided. Similarly, indices computed on the single proportions have a limited meaning because of the constraint to 100% – joint indices should be used instead.

Response: Thanks for the referee’s suggestion about the descriptive statistics for the original and log ratio transformed soil psf data, Component-wise medians were replaced with multivariate median based on depth measurements in the revised version of **Page 24, L13-L15**, and multivariate median method is available in the R package “depth”. Moreover, for some indices of the single proportions, univariate descriptive statistical assessment is widely used in data analysis of soil particle size fractions: the sum of the mean is 100 %, and SD, CV and MAD are used to describe the data stability; skewness and kurtosis are used to describe the data distribution. It is important, especially for machine-learning models which are modeled

independently in our study.

“Furthermore, multivariate median (median center in Table 2) based on depth measures (see Bedall and Zimmermann, 1979; Gower, 1974; Small, 1990) were used because of the sum-constraint of compositional soil psf data.”

Page 24, L21-26:

5 *“With respect to the original (untransformed) data of sand, the mean (30.64 %) was much higher than that of median center (26.06 %); conversely, both silt and clay were the opposite, with lower means (silt: 55.79 %, clay: 13.57 %) than median centers (silt: 59.51 %, clay: 14.43 %). For the log ratio transformed data, different log ratio approaches delivered the same means for sand, silt and clay, respectively. Additionally, the means of sand (28.69 %) and silt (60.54 %) were closer to the median centers of the original data, aside from clay, with a mean of 10.78 %.”*

10

Comment 8: P. 19 line 15: the methods on the original scale are designed in the Euclidean geometry, so there is no surprise in that they outperform methods developed to optimize other criteria (log-ratio geometry). The authors should better highlight the conceptual difference of working on the original scale or on the transformed scale.

15 **Response:** Thanks for the referee’s suggestion about the interpretation of the difference of the Aitchison (log-ratio) geometry and the Euclidean geometry. We focused on the interpretation of the conceptual difference of the Euclidean geometry (the original scale) and the Aitchison geometry (the transformed scale) in the revised version of **Page 44, L22-28**.

“Log ratio approaches can overcome the “closure effect”, spurious correlation and negative bias of compositional data, and the transformed data will be more symmetric and follow a normal distribution (Odeh et al., 2003; Wang and Shi, 2017). However, the indicators and methods on the original scale were designed in the Euclidean geometry. Thus, there has been a concern in log ratio approaches that the optimal estimate of log ratio transformed data does not deliver the optimal estimate of the compositions back-transformed to the real space, which leads to the result that the ORI approach outperformed those in log-ratio geometry.”

20

Comment 9: Table 2: I’m not sure it is meaningful to provide information on single part if the analysis – as I understood – was performed as to ensure that the total is 100%. I think it would be more meaningful and appropriate to display the overall RMSE, MAE and R² (sum of the element-wise numbers) – in the same way as AD is just one value for the Aitchison distance between compositional vectors.

25

Response: Thanks for the referee’s question about overall indicators of comparison of machine-learning models combined with different transformed data. There is widely used to calculate the single part of indicators (i.e. RMSE, MAE, R²) in many previous pieces of research of soil particle size fractions interpolation rather than the overall RMSE, etc. The results in our manuscript revealed the performance of component (sand, silt, and clay) were different when single indicators were considered. In fact, single fraction however was interested in spatial distribution in most cases. Further, the overall indicators cannot be added up such as R² due to the limitation of range (0 to 100 %). To overcome the disadvantages of these indices, AD and

30

STRESS were used in our study to provide more meaningful comparisons for compositional data as overall indicators of all components. However, in our opinion, analysis of single fraction should not be ignored for systematic comparisons in our study.

5 **Comment 10: P. 30: the authors discuss their results in comparison with previous ones. They should however discuss whether these differences are due to the particular case study considered or if they can be considered of more general validity.**

Response: Thanks for the referee's suggestion about a comparison of results with previous researches and further discussion. We paid more attention to the cause of different results from the perspective of soil sampling data, model uncertainty and the scale of the study area in the revised version of **Page 43, L20-L25**.

10 *"For more general validity, soil psf sampling data and the range of study area should be taken into account. In our study, data did not follow normal distribution, even the log ratio approaches were employed, and p values were not significant in k-s test; additionally, spatial prediction of soil psf and soil texture based on machine-learning methods were applied for not only a large amount of soil sampling data but also regional scale study area. From this point of view, our consequences therefore*
15 *could provide more general evidence to other researches."*

Comment 11: There are several typos and sentences to be revised in terms of English wording; I suggest a careful revision.

Response: Thanks for the referee's suggestion about the English words in our manuscript. We have improved the overall language of this article and we have checked and improved the writing in the revised version.

Reference

- Abdi, D., Cade-Menun, B. J., Ziadi, N., and Parent, L. E.: Compositional statistical analysis of soil p-31-nmr forms, *Geoderma*, 257, 40-47, 10.1016/j.geoderma.2015.03.019, 2015.
- 25 Aitchison, J.: The statistical-analysis of compositional data, *Journal of the Royal Statistical Society Series B-Methodological*, 44, 139-177, 1982.
- Aitchison, J.: On criteria for measures of compositional difference, *Mathematical Geology*, 24, 365-379, <https://doi.org/10.1007/bf00891269>, 1992.
- Aitchison, J.: The one-hour course in compositional data analysis or compositional data analysis is simple, 1997.
- 30 Bedall, F. K., and Zimmermann, H.: Algorithm as 143: The mediancentre, *Journal of the Royal Statistical Society. Series C (Applied Statistics)*, 28, 325-328, 10.2307/2347218, 1979.
- Buchanan, S., Triantafilis, J., Odeh, I. O. A., and Subansinghe, R.: Digital soil mapping of compositional particle-size fractions using proximal and remotely sensed ancillary data, *Geophysics*, 77, WB201-WB211, 10.1190/geo2012-0053.1, 2012.

- Burrough, P. A., van Gaans, P. F. M., and Hootsmans, R.: Continuous classification in soil survey: Spatial correlation, confusion and boundaries, *Geoderma*, 77, 115-135, [https://doi.org/10.1016/S0016-7061\(97\)00018-9](https://doi.org/10.1016/S0016-7061(97)00018-9), 1997.
- Butler, J. C.: Effects of closure on the moments of a distribution, *Journal of the International Association for Mathematical Geology*, 11, 75-84, 10.1007/bf01043247, 1979.
- 5 Deng, X. F., Chen, X. J., Ma, W. Z., Ren, Z. Q., Zhang, M. H., Grieneisen, M. L., Long, W. L., Ni, Z. H., Zhan, Y., and Lv, X. N.: Baseline map of organic carbon stock in farmland topsoil in east china, *Agric. Ecosyst. Environ.*, 254, 213-223, 10.1016/j.agee.2017.11.022, 2018.
- Egozcue, J. J., Pawlowsky-Glahn, V., Mateu-Figueras, G., and Barcelo-Vidal, C.: Isometric logratio transformations for compositional data analysis, *Mathematical Geology*, 35, 279-300, <https://doi.org/10.1023/a:1023818214614>, 2003.
- 10 Egozcue, J. J., and Pawlowsky-Glahn, V.: Groups of parts and their balances in compositional data analysis, *Math. Geol.*, 37, 795-828, 10.1007/s11004-005-7381-9, 2005.
- Gower, J. C.: Algorithm as 78: The mediancentre, *Journal of the Royal Statistical Society. Series C (Applied Statistics)*, 23, 466-470, 10.2307/2347150, 1974.
- Grunsky, E. C.: The interpretation of geochemical survey data, *Geochemistry: Exploration, Environment, Analysis*, 10, 27, 15 10.1144/1467-7873/09-210, 2010.
- Hijazi, R., and Jernigan, R.: Modelling compositional data using dirichlet regression models, 77-91 pp., 2009.
- Lark, R. M., and Bishop, T. F. A.: Cokriging particle size fractions of the soil, *European Journal of Soil Science*, 58, 763-774, <https://doi.org/10.1111/j.1365-2389.2006.00866.x>, 2007.
- Martin-Fernandez, J. A., Olea-Meneses, R. A., and Pawlowsky-Glahn, V.: Criteria to compare estimation methods of regionalized compositions, *Mathematical Geology*, 33, 889-909, <https://doi.org/10.1023/a:1012293922142>, 2001.
- Niang, M. A., Nolin, M. C., Jegou, G., and Perron, I.: Digital mapping of soil texture using radarsat-2 polarimetric synthetic aperture radar data, *Soil Sci. Soc. Am. J.*, 78, 673-684, 10.2136/sssaj2013.07.0307, 2014.
- Odeh, I. O. A., Todd, A. J., and Triantafyllis, J.: Spatial prediction of soil particle-size fractions as compositional data, *Soil Science*, 168, 501-515, <https://doi.org/10.1097/00010694-200307000-00005>, 2003.
- 25 Reimann, C., and Filzmoser, P.: Normal and lognormal data distribution in geochemistry: Death of a myth. Consequences for the statistical treatment of geochemical and environmental data, *Environmental Geology*, 39, 1001-1014, <https://doi.org/10.1007/s002549900081>, 2000
- Small, C. G.: A survey of multidimensional medians, *International Statistical Review*, 58, 263-277, 10.2307/1403809, 1990.
- Streiner, D. L.: Maintaining standards: Differences between the standard deviation and standard error, and when to use each, 30 *Canadian Journal of Psychiatry-Revue Canadienne De Psychiatrie*, 41, 498-502, 10.1177/070674379604100805, 1996.
- Wang, Z., and Shi, W.: Mapping soil particle-size fractions: A comparison of compositional kriging and log-ratio kriging, *Journal of Hydrology*, 546, 526-541, <https://doi.org/10.1016/j.jhydrol.2017.01.029>, 2017.

Systematic comparison of five machine-learning methods in classification and interpolation of soil particle size fractions using different transformed data

Mo Zhang^{1,2}, Wenjiao Shi^{1,3}

5 ¹Key Laboratory of Land Surface Pattern and Simulation, Institute of Geographic Sciences and Natural Resources Research, Chinese Academy of Sciences, Beijing 100101, China

²School of Earth Sciences and Resources, China University of Geosciences, Beijing 100083, China

³College of Resources and Environment, University of Chinese Academy of Sciences, Beijing 100049, China

Correspondence to: Wenjiao Shi (shiwj@lreis.ac.cn)

10 **Abstract.** Soil texture and soil particle size fractions (psf) play an increasing role in physical, chemical and hydrological processes. Digital soil mapping using machine-learning methods was widely applied to generate a more detailed prediction of qualitative or quantitative outputs than traditional soil-mapping methods in soil science. As compositional data, interpolation of soil psf combined with log ratio approaches was developed to improve the prediction accuracy, which also can be used to indirectly derive soil texture. However, few reports systematically analyzed and compared the classification and regression, 15 the ~~accuracy~~accuracy of original (untransformed) and log ratio approaches, and the performance of direct and indirect soil texture classification using machine-learning methods. In this total, a total of 45 evaluation models generated from five different machine-learning models combined with original and three log ratio approaches—additive log ratio, centered log ratio and isometric log ratio (ALR, CLR and ILR, respectively), to evaluate and compare the performance of soil texture classification and soil psf interpolation. The results demonstrated that log ratio approaches modified the soil sampling data 20 more symmetrically, and with respect to soil texture classification, random forest (RF) and extreme gradient boosting (XGB) showed notable consequences. For soil psf interpolation, RF delivered the best performance among five machine-learning models with lowest root mean squared error (RMSE, sand: 15.09 %, silt: 13.86 %, clay: 6.31 %), mean absolute error (MAE, sand: 10.65 %, silt: 9.99 %, clay: 5.00 %), Aitchison distance (AD, 0.84) and standardized residual sum of squares (STRESS, 0.61), and highest coefficient of determination (R^2 , sand: 53.28 %, silt: 45.77 %, clay: 53.75 %). STRESS was improved using 25 log ratio approaches, especially CLR and ILR. There is a pronounced improvement (21.3 %) in the kappa coefficient using indirect soil texture classification compared to the direct approach. Our systematic comparison helps to elucidate the processing and selection of compositional data in the spatial simulation.

1 Abbreviations: psf, soil particle-size fractions; HRB, Heihe River Basin; DSM, digital soil mapping; KNN, k-nearest neighbor; MLP, multilayer perceptron neural network; RF, random forest; SVM, support vector machines; XGB, extreme gradient boosting; ALR, additive log-ratio; CLR, centered log-ratio; ILR, isometric log-ratio; ORI, original; ~~ROC, receiver operating characteristics~~; PRC, precision-recall ~~curve~~; ~~AUC, area under the ROC curve~~; AUPRC, area under the PRC;

1 Introduction

Soil texture, classified by ranges of soil particle-size fractions (psf), is one of the most important attributes affecting the soil properties and the physical, chemical and hydrological processes covering soil porosity, soil fertility, water retention, infiltration, drainage and aeration. Measuring soil texture can be used for soil fertility management (Pahlavan-Rad and Akbarimoghaddam, 2018), water management (Thompson et al., 2012), maintenance of organic carbon (Bationo et al., 2007) and provision of ecosystem services (Adhikari and Hartemink, 2016). The soil psf, i.e., sand, silt and clay, are vital in most hydrological, ecological, and environmental risk assessment models (Liess et al., 2012). The spatial distributions of soil texture and soil psf affect and control runoff generation, slope stability, depth of accumulation and soluble salt content (McNamara et al., 2005; Follain et al., 2006; Yoo et al., 2006; Gochis et al., 2010; Crouvi et al., 2013).

Previous reports revealed that there are close correlations between the spatial variations of soil texture and landscape and topography (Gobin et al., 2001; Brown et al., 2004; Zhao et al., 2009; Liess et al., 2012). Compared with traditional soil mapping methods, digital soil mapping (DSM) has an obvious advantage in that it is considerably more economical and efficient; additionally, soil maps using DSM yielded more details because of the development of data-mining algorithms and GIS tools and more extensive application of spatial remote sensing data, particularly in the regional and continental scale. DSM methods were applied by an increasing number of soil scientists to map soil properties using ancillary data (McBratney et al., 2003; Zeraatpisheh et al., 2017), the so-called environmental covariates, which can be obtained from digital elevation models (DEM), remote sensing data, and categorical or geomorphology maps (Krasilnikov et al., 2011). Furthermore, some soil physicochemical attributes such as soil organic carbon (SOC) and pH, were also permissible to obtain as environmental covariates (Camera et al., 2017). Wang and Shi (2017) also recommended that the soil psf prediction should consider the ancillary data, which can enhance the performance of interpolation.

Different machine-learning methods, such as boosting regression trees (Jafari et al., 2014; Yang et al., 2016), random forests (Hengl et al., 2015; Zeraatpisheh et al., 2017) and artificial neural networks (Bagheri Bodaghabadi et al., 2015; Taalab et al., 2015), have been most commonly employed in DSM models for both regression and classification combined with environmental covariates in soil science. Hengl et al. (2015) contrasted the performance of spatial predictions of soil properties, such as soil psf, using random forests and linear regression, and the results demonstrated that the random forests were superior to the linear regression with remarkable advantages of not only robust to noise but also low bias and variance. Hengl et al.

RMSE, root mean squared error; MAE, mean absolute error; R^2 , coefficient of determination; MAD, median absolute deviation; AD, Aitchison distance; STRESS, standardized residual sum of squares; **SD, standard deviation, CV, coefficient of variation**; KNN_ALR, KNN_CLR, KNN_ILR, KNN_ORI, MLP_ALR, MLP_CLR, MLP_ILR, MLP_ORI, RF_ALR, RF_CLR, RF_ILR, RF_ORI, SVM_ALR, SVM_CLR, SVM_ILR, SVM_ORI, XGB_ALR, XGB_CLR, XGB_ILR, XGB_ORI, KNN, MLP, RF, SVM, XGB combined with ALR, CLR, ILR, ORI respectively; CiLo, clay loam; Lo, loam; LoSa, loamy sand; Sa, sand; SaCiLo, sandy clay loam; SaLo, sandy loam; Si, silt; SiCiLo, silty clay loam; SiLo, silt loam.

(2017) improved the prediction of organic carbon, bulk density, pH and soil texture fractions on a global scale using machine-learning models – random forest, gradient boosting and multinomial logistic regression – indicating that random forest and gradient boosting outperformed linear models in large data sets. Taghizadeh-Mehrjardi et al. (2015) investigated the predictive power of soil classes using six machine learning-based classifiers and found that artificial neural network and decision trees performed better than any other models they mentioned with relatively high overall [accuracy](#) and kappa coefficients. Heung et al. (2016) evaluated a suite of 10 machine-learning models for predicting soil taxonomic units, and the consequences suggested that although the k-nearest neighbor and support vector machine had the highest accuracy, “tree learners” were preferred because of the interpretability of the results and the speed of parameterization. Most previous studies selected one or more machine-learning algorithms to simulate soil category or continuous variables for classification or regression problems. From this perspective, however, few studies systematically analyzed both soil texture classification and soil psf interpolation using multiple machine-learning methods.

The soil psf, which can be classified as soil texture, are not only continuous variables but also compositional data. We need to pay more attention to the latter case. Numerous different interpretations of the interpolation of compositional data in soil science have been suggested (Gobin et al., 2001; Lark and Bishop, 2007; Salazar et al., 2015), and the most extensively used were a combination of log ratio approaches involving the additive log ratio (ALR) and the centered log ratio (CLR) put forward by Aitchison (1982), as well as the isometric log ratio (ILR) from Egozcue et al. (2003). However, most studies using log ratio approaches to simulate the spatial variation of soil psf were kriging methods (so-called geostatistics), rather than machine-learning methods. Huang et al. (2014) combined multiple linear regression with ALR to improve the prediction precision of soil psf using electromagnetic data on a 1-m transect. Odeh et al. (2003) proposed that modified ALR ordinary kriging transcended compositional kriging and cokriging. Sun et al. (2014) contradistinguished compositional kriging, log ratio cokriging, cokriging, and ALR-cokriging, and produced proximate results. In contrast, Walvoort and de Gruijter (2001) thought compositional kriging had better performance than ALR ordinary kriging. Zhang et al. (2013) suggested compositional kriging was more appropriate for soil texture prediction than symmetry log ratio ordinary (or regression) kriging. Wang and Shi (2018) developed log ratio kriging combined with robust variogram estimation, which was preferable to compositional kriging methods. However, few studies combined log ratio with machine-learning models for soil psf interpolation in soil science. Aside from those mentioned above, the lack of systematic comparison of accuracy, strengths and weaknesses between original (untransformed) and log ratio approaches should be considered, especially in terms of combining with machine-learning methods.

Soil texture classification using machine-learning methods can be classified as a dependent variable; furthermore, it also can be derived indirectly from soil psf. Camera et al. (2017) reported that random forests were more remarkable than multinomial logistic regression in the direct soil texture classification. Wu et al. (2018) compared the support vector machines (SVM), artificial neural network (ANN), and classification tree (CT) models, demonstrating better prediction performance generated from SVM than from CT and ANN. For the indirect classification of soil texture, Poggio and Gimona (2017)

combined hybrid geostatistical generalized additive models with ALR and modeled soil particle classes at medium resolution (250 m) in Scotland, expecting that vegetation index, morphological features and information about the phenological season were of vital significance as environmental covariates. Considering the particularity of compositional data, the consequences of soil psf classification and regression (indirect soil texture classification and soil psf interpolation, respectively) could be compared from the direct and indirect soil texture classification as a result of the relationship between soil texture and soil psf. Nevertheless, few studies systematically compared these using different machine-learning methods combined with original (untransformed) and log ratio transformed data for both direct and indirect soil texture classification.

In our study, five machine-learning models – k-nearest neighbor (KNN), multilayer perceptron neural network (MLP), random forest (RF), support vector machines (SVM), and extreme gradient boosting (XGB) – were included and applied for DSM of soil texture classification and soil psf interpolation. Furthermore, the original (untransformed) and log ratio transformed data were also combined with the machine-learning algorithms mentioned above for soil psf interpolation. Hence, the objectives of this study are (i) to compare different performance of five machine-learning models in direct soil texture classification, (ii) to evaluate the [accuracy](#) of different log ratio approaches and original (untransformed) method applied for soil psf from the perspective of compositional data using machine-learning models, and (iii) to estimate whether the [accuracy](#) of indirect soil texture classification using original (untransformed) data and log ratio transformed data were improved compared with the direct soil texture classification.

2 Data and methods

2.1 Study area

The Heihe River Basin (HRB, 97 °6 '-102 °3 ' E, 37 °43 '~ 42 °40 ' N) is situated in the Hexi Corridor, northwest of China, covering the Inner Mongolia Autonomous Region, Gansu and Qinghai provinces (Fig. 1a), which is the second largest inland river basin in China with an area of 146,700 km². The elevation and three reaches (i.e., upper, middle and lower) of the study area are shown in Fig. 1b. For the upper reaches of HRB, the climate changes significantly with altitude; the mean annual precipitation is 350 mm, the mean annual temperature is from -5-4 °C and the annual average evaporation is 1000 mm. For the middle reaches of HRB, the mean annual precipitation declines between 250 and 50 mm, the annual average evaporation increases from 2000 (east) to 4000 mm (west), and the mean annual temperature is from 2.8 to 7.6 °C. The lower reaches of HRB are situated in Ejina Banner on the Alxa Plateau, which is an arid desert climate with annual precipitation under 50 mm and annual average evaporation above 3500 mm; the mean annual temperature is from 8 to 10 °C.

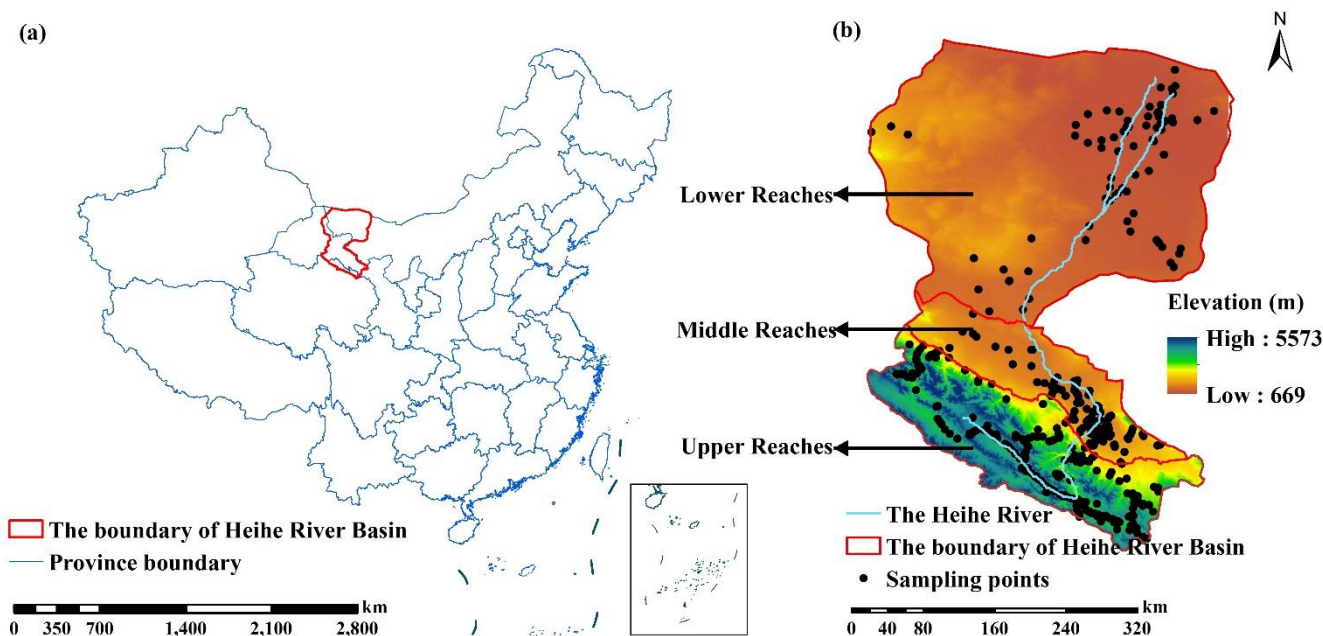


Figure 1. The (a) geographical location, (b) Heihe River, elevation and soil sampling points of Heihe River Basin, China.

The vegetation of the upper reaches of HRB is influenced from the southeast to northwest by hydrothermal conditions. The main vegetation types are alpine vegetation (4000-5000 m), alpine meadow vegetation belt (3000-4000 m), alpine shrub meadow (3200-3800 m), mountain forest meadow belt (2400-3200 m), mountain grassland belt (1800-2400 m), and desert base belt (less than 1800 m). The main vegetation types of the middle and lower reaches of the HRB are relatively fewer, including cultivated vegetation and desert, and the areas near the Heihe River on the lower reaches are shrub and steppe.

The main soil types are frigid desert soils (less more higher than 4000 m), alpine meadow soil and alpine steppe soil (3600-4000 m), gray cinnamon soil and chernozem (3200-3600 m), sierozem and chestnut soil (2600-3200 m), chestnut soil (2300-2600 m) and sierozem (1900-2300 m) on the upper reaches of the HRB. The main soil types on the middle reaches of HRB are aeolian sandy soil, frigid frozen soil and gray brown desert soil. The main soil types in the lower reaches of HRB are aeolian sandy soil, gray brown desert soil (northwest) and lithosol (northeast).

The main types of geomorphology on the upper reaches of HRB are modern glaciers, alpine and hilly, and intermountain basinplimatic basins. Narrow plains are distributed on the middle reaches of HRB. For the lower reaches, the main types of geomorphology are hilly (northwest), plain, sandy land and platform (east), and the area near Heihe River is a flood plain.

2.2 Soil sampling

A total of 640 soil sampling points was collected in the HRB from the Science Data Center of Cold and Arid Regions (WestDC) in China (<http://westdc.westgis.ac.cn/>), involving 392 soil sampling points on the upper reaches and 248 soil sampling points

on the middle and lower reaches of the HRB. The soil types, vegetation types, distribution of DEM and geomorphology types of the HRB were considered in soil sample collection according to the location and proportion of these types for the purpose of more representative spatial characteristics of soil psf using limited soil samples. There were more soil sampling points on the middle and upper reaches of HRB due to the more complicated soil types and vegetation types in these areas. In contrast, the types on the lower reaches are relatively similar with more desert in the northwest. Hence, the east of the lower reaches of the HRB contained more soil sampling points. All soil samples had information about soil psf (i.e., sand, silt and clay) and related environmental covariates using a laser diffraction approach and the extraction tool in ArcGIS, respectively, and the global position system (GPS) recorded the position information.

2.3 Environmental covariates and pre-processing

The environmental covariates, such as topographic attributes, remote sensing attributes, climate and position attributes, soil physicochemical attributes and categorical maps, are logically related to the distributions of soil psf. System for Automated Geoscientific Analysis (SAGA) GIS (Conrad et al., 2015) was used to compute ~~their~~the topographic attributes from DEM, including slope, aspect, convergence index, general curvature, plane curvature, profile curvature and valley depth. Remote sensing attributes, including the normalized difference vegetation index (NDVI, Huete et al., 2002), the Brightness index (BI, Metternicht and Zinck, 2003), and the soil adjusted vegetation index (SAVI, Huete, 1988) were derived from the Landsat 7 based on band operation. We also collected climate attributes from the National Meteorological Information Center (NMIC, <http://data.cma.cn/>), such as the mean annual precipitation and the mean annual temperature. Latitude and longitude were also considered because of the large scale of the HRB. Mean annual surface evapotranspiration data (Wu et al., 2012) were gathered from WestDC (<http://westdc.westgis.ac.cn/>), as ~~were well as~~ soil physicochemical attributes, such as soil organic carbon, saturated water content, field water holding capacity, wilt water content, saturated hydraulic conductivity, and soil thickness (Yi et al., 2015; Song et al., 2016; Yang et al., 2016), which can address the distributions of soil psf, as well. Additionally, the categorical maps were of significance, such as geomorphology types, soil types, land cover and vegetation types. For slope, the method of dividing the hierarchy rotates clockwise from the north (0°), and each 45° was an interval, including north (337.5-22.5°), northeast (22.5-67.5°), east (67.5-112.5°), southeast (112.5-167.5°), south (167.5-202.5°), southwest (202.5-247.5°), west (247.5-292.5°), and northwest (292.5-337.5°).

2.4 Machine learning methods and parameters optimization

2.4.1 K-nearest neighbor (KNN)

K-nearest neighbor (KNN) is a simple non-parametric classifier based on the known instance to label unknown instance (Cover and Hart, 1967). For the test set, k-nearest training set vectors were found, and maximum summed kernel densities were computed for classification. Moreover, continuous variables can also be predicted for regression with the average values of k-

nearest neighbors. Weighted KNN is an extended version of KNN that considers the distances of the nearest neighbors; therefore, the parameters of KNN contain the maximum value of k (kmax), the distances of the nearest neighbors (distance) and the types of a kernel function (kernel). The KNN model is available in the R package “kkn” (Schliep and Hechenbichler, 2016).

5 **2.4.2 Multilayer perceptron neural network (MLP)**

Multilayer perceptron neural network (MLP), which is currently one of the most popular multilayer ~~feed-forward~~feedforward backpropagation networks, was selected to train artificial neural network (ANN) models in our study due to its rapid operation, the small set of training requirements and ease of implementation (Subasi, 2007). MLP neurons can perform classification or regression depending on whether the response variable is categorical or continuous. The MLP has three sequential layers: input layer, hidden layer and output layer. The resilient backpropagation algorithm was chosen because the learning rate of this algorithm ~~is~~was adaptive, avoiding oscillations and accelerating the learning process (Behrens and Scholten, 2006). The range of the data set should be standardized because MLPs operate in terms of ~~the~~ scale 0 to 1. MLP can be run using the R package “RSNNS” (Bergmeir and Benitez, 2012).

15 **2.4.3 Random forest (RF)**

Random forest (RF) was developed by Breiman (2001), combining the bagging method (Breiman, 1996) with the random variable selection, and the principle was to merge a group of “weak learners” together to form a “strong learner”. Bootstrap sampling is used for each tree of RF, and the rules to binary split data are different for regression and classification problems. For classification, the Gini index is used to split the data; for regression, minimizing the sum of the squares of the mean deviations can be selected to train each tree model. Benefits of using RFs are that the ensembles of trees are used without pruning. In addition, RF is relatively robust to overfitting, and standardization or normalization ~~are~~is not necessary because it is insensitive to the range of value. Two parameters should be adjusted for the RF model: the number of trees (ntree) and the number of features randomly sampled at each split (mtry). The RF model is available in the R package “randomForest” (Liaw and Wiener, 2002).

20 **2.4.4 Support vector machines (SVM)**

25 The support vector machine (SVM), proposed by Cortes and Vapnik (1995), is a type of generalized linear classifier that is widely applied for classification and regression problems in soil science (Borges, 1998). The main principle of SVM is to classify different classes by constructing an optimal separating hyperplane in the feature space (so--called “structural risk minimization”). Regression problems also can be solved by minimization of the structural risk using loss functions (Vapnik, 1998) in SVM, named support vector regression. The advantages of SVMs are that they are effective in high dimensional

spaces. Radial basis function was selected for SVM as the kernel function in our study, and two other parameters need to be tuned, i.e., cost and gamma, controlling the tradeoff between the classification accuracy and complexity, and the ranges of radial effect, respectively. The SVM model is available in the R package “e1071” (Meyer et al., 2017).

2.4.5 Extreme gradient boosting (XGB)

5 Extreme Gradient Boosting, put forward by Chen and Guestrin (2016), is an efficient method of implementation for gradient
boosting frames, tree learning algorithms, and efficient linear model solvers to solve both classification and regression
problems (Chen et al., 2018). Like the boosted regression trees (Elith et al., 2008), it follows the principle of gradient
enhancement; however, more regularized model formalization is applied to XGB to control over-fitting, making it more
10 remarkable. In addition, parallel calculations can be automatically executed during the training phase of the XGB model,
presenting a great advantage in large data sets, as the XGB can be more than ten times faster than the existing gradient boosting
model (Chen and Guestrin, 2016). There are seven parameters should be tuned in XGB, containing the learning rate (eta), the
maximum depth of a tree (max_depth), the max number of boosting iterations (nrounds), the subsample ratio of columns
(colsample_bytree), the subsample ratio of the training instance (subsample), the minimum loss reduction (gamma) and the
15 minimum sum of instance weight (min_child_weight). The XGB model is available in the R package “xgboost” (Chen et al.,
2018).

2.4.6 Parameters optimization

The parameters of machine-learning models we mentioned above need to be adjusted, and the numbers of these parameters
of models are different. For instance, XGB has seven parameters and is one of the most complicated models; on the other hand,
for the MLP, in the case where we have chosen the algorithm, the only parameter that should be tuned is the size of the MLP
20 model.

R package “caret” (Kuhn, 2018) provides an effective grid-search method that can automatically adjust the parameters by
setting the adjustment grid, avoiding the uncertainty of artificial adjustment for some models (e.g., XGB) with more parameters.
A set of parameters with the lowest RMSE or the highest R^2 for regression and the highest overall accuracy or kappa coefficient
for classification by cross-validation can be selected to be the best parameters. However, in the presence of many adjustment
25 parameters, it may be inefficient due to the long training time. Thus, we used the other package of “randomForest” for RF and
“kknn” for KNN, which can also restructure the parameters for these two models.

In our study, eleven dependent variables (i.e., ten for regression and one for classification) were trained with environmental
covariates (independent variables) for the sake of parameter adjustment for each model, including “sand, silt, clay, ilr1, ilr2,
alr1, alr2, clr1, clr2, clr3” and “class”. Subsequently, the parameters were definitely computed; here, we just give the relative
30 ranges of the parameters after adjustment for most dependent variables; for example, in KNN, the kmax was 15, the distance
was 1, and the kernel was rectangular; in MLP, the size fluctuated between 5 and 10; in RF, the ntree was 1000 and mtry

fluctuated from 9 to 11; in SVM, gamma was 0.01 and cost was 1; and in XGB, the range of parameters of max_depth (3-4), eta (0.05-0.1), colsample_bytree (0.6-0.8), nrounds (30), subsample (0.8-1), gamma (0-0.4), and min_child_weight (0.6-0.8) were obtained after conditioning.

2.5 Log-ratio transformation methods

5 For soil psf compositional data (i.e. sand, silt and clay), the sum of the components is 1 (or 100 %), which should be guaranteed. Soil ~~particle size~~ data, including three dimensions, are typical compositional data. The closed number system can be explained as follows: the individual variables in the data set are not independent of each other; moreover, they are related by being expressed as a percentage (Filzmoser et al., 2009). ~~In the Euclidean space, one dimension (variable) would be omitted. As compositional data, it is not common for the original method soil particle size fractions (i.e. sand, silt and clay) to guarantee no information loss follow normal distribution (Lark and Bishop, 2007); moreover, because of the constant sum constraint. Therefore, the spurious correlations between components, different consequences would occur on different measurement scales, which makes more complicated interpretation (Abdi et al., 2015; Reimann and Filzmoser, 2000). Some significant principles such as scale invariance, sub-compositional coherence and dominance of compositions (Aitchison, 1997) should be taken into account in the compositional analysis. Indicators and statistical methods defined in the Euclidean geometry or based on Euclidean space is not appropriate for the analysis of soil psf data, distances could reveal misleading or biased consequence (Butler, 1979) such as mean, median, standard deviation, standard PCA, analysis of the (co)variance, etc.~~ The most widely used approaches ~~are were so-called~~ log ratio ~~approaches transformation~~ (Aitchison, 1982), ~~consisting of and~~ the additive log ratio, centered log ratio and isometric log ratio (ALR, CLR and ILR for short, respectively) from Aitchison (1982) and Egozcue et al. ~~(2003) can be used to operate within the log-ratio approaches by simply using the Euclidean geometry on the transformed data.~~ For the composition of D ~~elements~~ $x = [x_1, \dots, x_D]$, $x_j > 0$, $\forall j = 1, \dots, j-1, j+1, \dots, D$, and $\sum_{j=1}^D x_j = 1$, the transformation equation for ALR is defined as follows:

$$alr(x) = (\ln \frac{x_1}{x_j}, \dots, \ln \frac{x_{j-1}}{x_j}, \ln \frac{x_{j+1}}{x_j}, \dots, \ln \frac{x_D}{x_j}), \quad (1)$$

For soil psf ($D = 3$) in our study, the transformation equations for ALR are:

$$alr(1) = \ln \frac{\text{sand}}{\text{clay}}, \quad (2)$$

$$25 \quad alr(2) = \ln \frac{\text{silt}}{\text{clay}}, \quad (3)$$

All of the information regarding the soil psf was contained in ~~alr(1) and alr(2)~~ Eq. (2) and Eq.(3); however, the ALR has been criticized because the choice of the denominator is subjective, which can influence the results (~~Bacon Shone, 2011~~ Aitchison, 1982). The CLR transformation method can remove this arbitrariness, and the equation is defined as follows

$$clr(x) = (y_1, \dots, y_j, \dots, y_D) = (\ln \frac{x_1}{\sqrt{\prod_{j=1}^D x_j}}, \dots, \ln \frac{x_D}{\sqrt{\prod_{j=1}^D x_j}}), \quad (4)$$

30 where y_j is the j th component. Similarly, for the soil psf, the transformation equations for CLR are:

$$clr(1) = \ln \frac{sand}{\sqrt[3]{sand \times silt \times clay}}, \quad (5)$$

$$clr(2) = \ln \frac{silt}{\sqrt[3]{sand \times silt \times clay}}, \quad (6)$$

$$clr(3) = \ln \frac{clay}{\sqrt[3]{sand \times silt \times clay}}, \quad (7)$$

In the CLR transformation method, the geometric mean composed of all compositions of soil psf is the denominator, and one-to-one mapping of equations and soil psf could be implemented. Nevertheless, the ~~CLR is inapplicable for multivariate analysis because the~~ sum of the dimensions of CLR is 0, ~~and thus the results are~~ the problem of spurious correlation is still present (i.e. collinear). These problems can be overcome by using ILR, which transforms all the information into $D-1$ orthogonal log contrasts (Abdi Egozcue et al., 2015, 2003). The transformation equations for ILR are defined as follows:

$$z = (z_1, \dots, z_{D-1}) = ilr(x), \quad (8)$$

$$z_i = \sqrt{\frac{D-i}{D-i+1}} \ln \frac{x_i}{\sqrt[3]{\prod_{j=i+1}^D x_j}}, \quad (9)$$

where z_i is the i th component. The ILR transformation equations for soil psf in our study can also be defined as follows:

$$ilr(1) = \sqrt{\frac{2}{3}} \ln \frac{sand}{\sqrt{silt \times clay}}, \quad (10)$$

$$ilr(2) = \sqrt{\frac{1}{2}} \ln \frac{silt}{clay}, \quad (11)$$

For a more uniform comparison of the descriptive statistics, the ordering of three components of soil psf followed sand-silt-clay, and we added the third equation for the ALR and ILR. Although all the information could be included in the first two equations, note that in the process of ~~interpolation model training~~, only the first two equations were used for ALR and ILR:

$$alr(3) = \ln \frac{clay}{sand}, \quad (12)$$

$$ilr(3) = \sqrt{\frac{2}{3}} \ln \frac{clay}{\sqrt{sand \times silt}}, \quad (13)$$

The equations for ~~alr(1), alr(2), alr(3)~~ Eq. (2), Eq. (3) and Eq. (12) were equivalent to ~~alr(sand), alr(silt), alr(clay)~~ alr(sand), alr(silt) and alr(clay) in ALR, the same as ~~in~~ ILR. The ~~back transformed inverse transformation~~ equations for ALR, CLR and ILR were recommended in ~~our previous their~~ research (Wang and Shi, 2017; Aitchison, 1992; Egozcue et al., 2005), and ~~were can be~~ computed in the “compositions” R package (van den Boogaart and Tolosana-Delgado, 2008). For the original (untransformed) method, the standardization function was used to ensure predictions of soil psf were between 0 and 100 and that their sum was 100%:

$$sand_s = \frac{sand}{(sand + silt + clay)} \times 100, \quad (14)$$

where, $sand_s$ is the content of sand after standardization, the same as silt and clay components.

2.6 Validation

2.6.1 Validation method

A total of 45 methods that we simulated used are were presented in Table 1; five machine-learning models were combined with one original (ORI) and three log ratio approaches (ALR, CLR, ILR). Five machine-learning methods were applied for direct soil texture classification; additionally, these methods were combined with original (untransformed) and log ratio transformed data for a total of 40 methods for indirect soil texture classification (20) and soil psf interpolation (20). The data were randomly divided into two sets to guarantee prediction accuracy; for instance, one (70 % = 448 soil samples) was employed for training models and the other (30 % = 192 soil samples) was set aside for validation. This process was repeated 30 times for soil texture classification and soil psf interpolation, and different indicators were chosen to evaluate different performances of models (or methods).

Table 1. The method system of soil texture classification and soil psf interpolation.

Methods	Soil texture classification		Soil psf interpolation
	Direct classification	Indirect classification	—
Original data (ORI)	KNN, MLP, RF, SVM, XGB	KNN_ORI, MLP_ORI, RF_ORI, SVM_ORI, XGB_ORI	
Log-ratio transformed data (ALR, CLR, ILR)	—	KNN_ALR, KNN_CLR, KNN_ILR, MLP_ALR, MLP_CLR, MLP_ILR, RF_ALR, RF_CLR, RF_ILR, SVM_ALR, SVM_CLR, SVM_ILR, XGB_ALR, XGB_CLR, XGB_ILR,	

2.6.2 Validation indicators for soil texture classification

The overall accuracy (Brus et al., 2011) and the kappa coefficient were selected to evaluate the overall effects of soil texture types predicted by different models. Moreover, the receiver operating characteristic (ROC) curve, precision-recall curve (PRC), area under the ROC curve (AUC), area under the precision-recall curve (AUPRC) and abundance index were applied to evaluate the performance of different soil texture types. The overall accuracy represents all samples of soil texture types correctly classified by machine-learning models, divided by the total number of samples of soil texture types used in the validation. The higher overall accuracy, the more accurate soil map (Brus et al., 2011):

$$\text{Overall Accuracy} = \frac{TP+TN}{TP+TN+FP+FN}, \quad (15)$$

where T, F, P and N denote True, False, Positive, and Negative and TP, TN, FP, FN were true positive, true negative, false positive, and false negative, respectively. When the numbers of samples in different classes are imbalanced in the data set, the

kappa coefficient can explain the agreement of classes (Marchetti et al., 2011), which is calculated based on the confusion matrix, the equation is defined as:

$$kappa = \frac{p_o - p_e}{1 - p_e}, \quad (16)$$

where, p_o is the probability of observed agreement (overall accuracy) and p_e is the probability of agreement when two classes are unconditionally independent. The strength of the kappa coefficients is interpreted in the following manner: 0.01-0.20: slight, 0.21-0.40: fair, 0.41-0.60: moderate, 0.61-0.80: substantial, 0.81-1.00: almost perfect (Landis and Koch, 1977). The probabilities of different soil texture types (sum to 1) obtained during the training and predicting processes of machine-learning models were selected to calculate the ~~sensitivity, specificity,~~ precision and recall, which indicated the extent of identifying positive cases:

$$Sensitivity = rRecall = \frac{TP}{TP+FN}, \quad (17)$$

$$Specificity = \frac{TN}{TN+FP}, \quad (18)$$

$$Precision = \frac{TP}{TP+FP}, \quad (18)$$

~~In general, sensitivity, precision and recall indicate the extent of identifying positive cases, and specificity demonstrates the extent of identifying the negative cases of models. ROC analysis is commonly used in two class problems. However, soil texture types are more than two classes. In our point of view, a one vs rest strategy was employed to produce different ROC graphs for each soil texture type.~~

$$P_i = c_i, \quad (20)$$

$$N_i = \cup j \neq i c_j \in C, \quad (21)$$

~~where C is the set including all classes, P_i is the positive class, N_i is the negative class, including all classes except c_i in ROC graph i (Fawcett, 2006).~~

~~In practice, the weakness of the ROC curve is that it cannot indicate the differences among the models in the cases of imbalanced samples between positive and negative. Soil texture data are a class-imbalanced data set of positive and negative, and the negative classifier would be overvalued under these circumstances because of the overabundance of majority (negative) examples, additionally revealing overly optimistic findings (Davis and Goadrich, 2006). However, precisionPrecision and recall curves (PRC_s) are more informative than ROC curves in dealing with class-imbalanced data (Fu et al., 2017). The R package “precrec” (Saito and Rehmsmeier, 2017) can generated ROC and PRC_s curves and computed AUC and AUPRC for each soil texture type. This process was repeated 30 times and eventually, the average ROC and PRC-PRC_s curves with their average areas under these curves were obtained. Similarly, confusion index (COI) based on prediction probability was calculated to evaluate the uncertainties of machine-learning models of classification (Burrough et al., 1997), which equation was as follows:~~

$$COI = [1 - (P_{max,i} - P_{secmax,i})], \quad (19)$$

where $P_{max,i}$ refers to the maximum value of probability at the position i and $P_{secmax,i}$ represents the second highest value of probability at the position i , the lower COI, the better performance of model. Abundance index was applied to describe the proportion of all soil texture types and well-classified soil texture types in the prediction map, which was defined as follows:

$$Abundance\ index = p/t, \quad (20)$$

- 5 where pp is all soil texture types in the prediction map and tt is well-classified soil texture type(s) in test sets. For the sake of ensuring the balance of the soil texture types, all nine soil texture types were involved in test sets, covering clay loam (CILo: 12), loam (Lo: 57), loamy sand (LoSa: 18), sand (Sa: 23), sandy clay loam (SaCILo: 4), sandy loam (SaLo: 58), silt (Si: 31), silty clay loam (SiCILo: 37), and silt loam (SiLo: 400); most were SiLo (62.5%) and the fewest were SaCILo (0.63%).

2.6.3 Validation indicators and uncertainty assessment for soil psf interpolation

- 10 The accuracy and performance of machine-learning models mentioned above for the original (untransformed) and different log ratio transformation approaches were evaluated using five statistical indicators, containing coefficient of determination (R^2), root mean square error (RMSE), mean absolute error (MAE), Aitchison distance ($AD_{\bar{y}}$) (Aitchison, 1992), and standardized residual sum of squares (STRESS)_F (Martin-Fernandez et al., 2001). [For the assessment of model uncertainty, the standard deviation \(SD\) and the ranges of 95 % confidence interval \(CI\) \(Streiner, 1996\) of indicators derived from running](#)
 15 [models 30 times were generated as indicators of prediction uncertainties.](#) The equations for the validation indicators R^2 , RMSE, MAE, AD and STRESS are as follows:

$$R^2 = \frac{\sum_{i=1}^n (Y_{i,m} - Y_{i,e})^2}{\sum_{i=1}^n (Y_{i,m} - \bar{Y}_{i,m})^2}, \quad (21)$$

$$RMSE = \sqrt{\frac{1}{n} \sum_{i=1}^n (Y_{i,m} - Y_{i,e})^2}, \quad (22)$$

$$MAE = \frac{1}{n} \sum_{i=1}^n |Y_{i,m} - Y_{i,e}|, \quad (23)$$

- 20 where $Y_{i,m}$, $Y_{i,e}$, $\bar{Y}_{i,m}$ and n are the measured, predicted and the mean of measured soil psf and the number of observations (soil sampling points for validation). Closer to 1 and higher values of R^2 and the lower values of RMSE and MAE show better performance of models and methods.

$$AD = \left[\sum_{i=1}^D \left[\log \frac{x_i}{g(x)} - \log \frac{X_i}{g(X)} \right]^2 \right]^{1/2}, \quad (24)$$

$$STRESS = \left[\frac{\sum_{i < j} (AD_{x,ij} - AD_{X,ij})^2}{\sum_{i < j} (AD_{x,ij})^2} \right]^{1/2}, \quad (25)$$

- 25 where x is the observed value; X is the predicted value; D is the number of dimensions (for soil psf is 3); $g(x)$ denotes the geometric mean $(x_1 \dots x_D)^{1/D}$; $AD_{x,ij}$ and $AD_{X,ij}$ are the ADs between the observed soil psf and the predicted soil psf at sites i and j . Both present that model performances are better when the values are lower.

2.6.4 Indirect soil texture classification by soil psf interpolation

Seventy percent of the 640 soil sampling points were used for training each machine-learning model, and the remaining 30 % were used for the soil psf interpolation; thereafter, we transformed the content of three components (sand, silt and clay) into the soil texture types in the USDA soil texture classification using the R package “soiltexture” (Moeys, 2018). Eventually, the overall accuracy and kappa coefficient were computed and evaluated. This process was repeated 30 times, and the averages of these consequences were employed to compare the classification performance ~~of for~~ each model. The direct and indirect soil texture classifications were also compared with the overall accuracy and kappa coefficient. The training and testing sets for each time were the same by setting seeds, and all calculations and analysis were performed with the freely available software R (R Core Team, 2018).

2.7 Statistical analysis for the original and log₋ratio transformed data

The ~~standard deviation (SD), coefficient of variation (CV), mean, median,~~ minimum (Min), maximum (Max), median absolute deviation (MAD), skewness (Skew), kurtosis and Kolmogorov-Smirnov test ($p>0.05$) were employed for descriptive statistical analysis of the original (untransformed) and log ratio transformed soil psf data. ~~The arithmetic mean of log- Furthermore, multivariate median (median center in Table 2) based on depth measures (see Bedall and Zimmermann, 1979; Gower, 1974; Small, 1990) were used because of the sum-constraint of compositional soil psf data. The arithmetic mean of log~~ ratio transformation data should be back-transformed to the original space. For $X = [X_1, \dots, X_n]$, the MAD can be calculated according to the Eq. (2826) as below:

$$MAD(X) = \text{median}(|X_i - \text{median}(X)|). \quad (26)$$

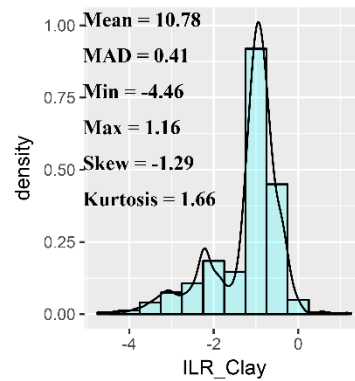
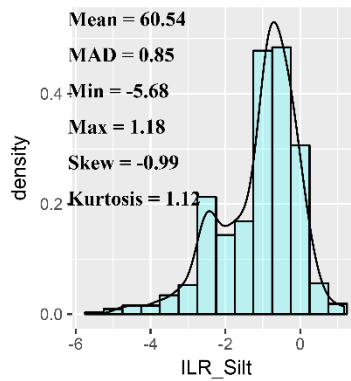
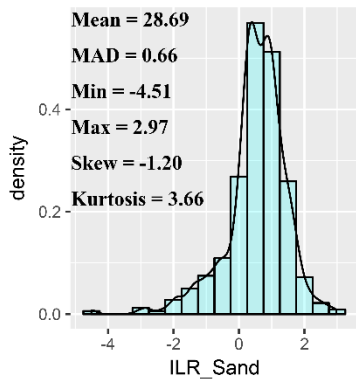
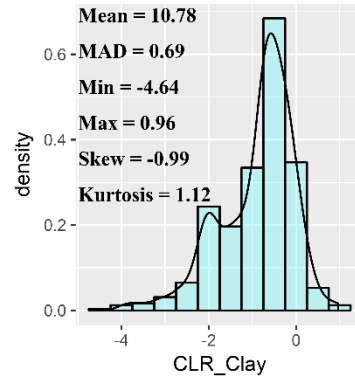
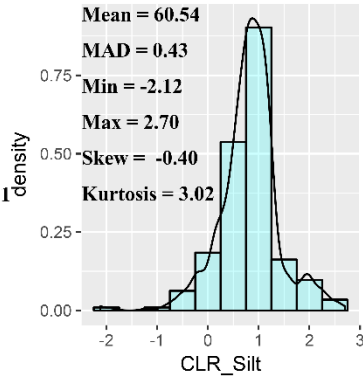
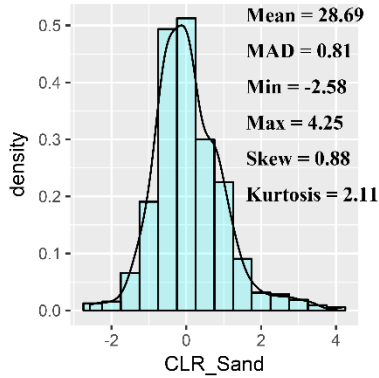
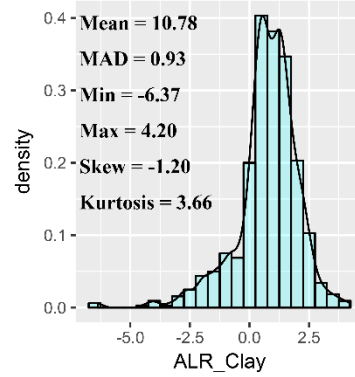
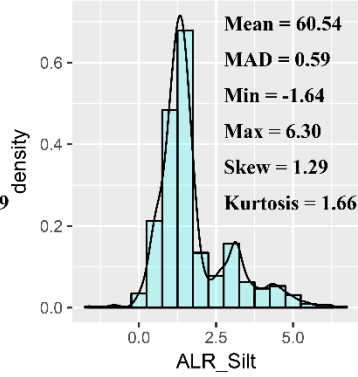
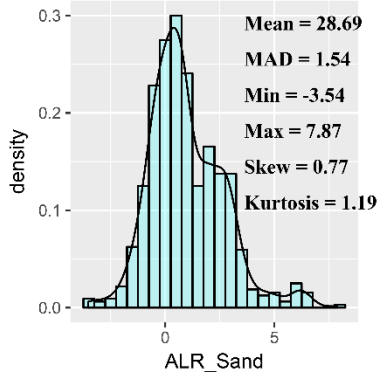
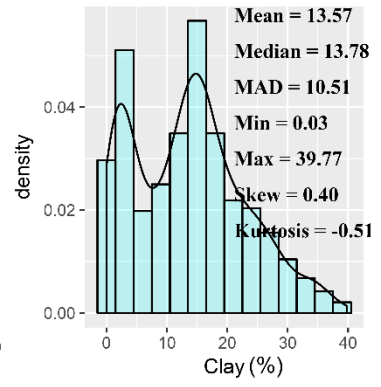
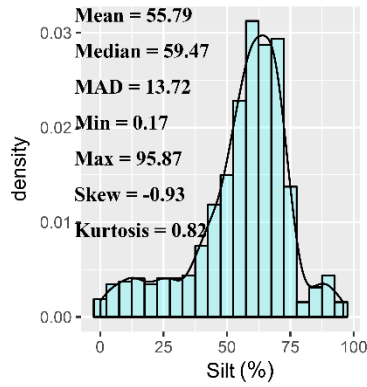
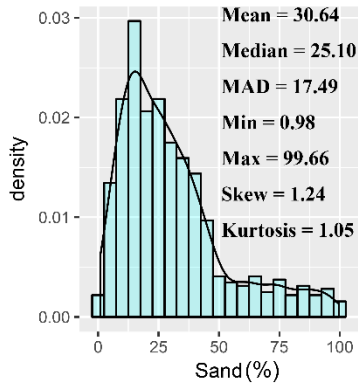
3 Results

3.1 The descriptive statistics for the original and log₋ratio transformed soil psf data

With respect to the original (untransformed) data of sand, the mean ~~fraction~~ (30.64 %) was much higher than that of median ~~fraction~~ ~~(25.10)~~ center (26.06 %); conversely, both silt and clay were the opposite, with lower ~~mean fractions~~ ~~means~~ (silt: 55.79 %, clay: 13.57 %) than median ~~fractions~~ centers (silt: 59.4751 %, clay: ~~13.78~~ 14.43 %). For the log ratio transformed data, ~~different log ratio approaches delivered the same means for sand, silt and clay, respectively. Additionally,~~ the means of sand (28.69 %) and silt (60.54 %) were closer to the median ~~values~~ centers of the original data, aside from clay, with a mean of 10.78 %. For standard deviation (SD) and coefficient of variation (CV), soil psf data in log ratio geometry had more stability and less variability compared with the original data.

All MADs of log ratio transformed data were much smaller than those of the original data in all cases; for instance, ILR contained the best value of MAD for sand (0.66) and clay (0.44), and CLR generated the lowest MAD for silt (0.43) among

different log ratio approaches (~~Fig.~~Table 2). All log ratio approaches had lower skews (ALR: 0.77, CLR: 0.88, ILR: -1.20) than those of the original data (1.24) ~~for-of~~ sand. ~~Moreover; moreover~~, CLR (-0.4) declined the original skew (-0.93) ~~for-of~~ silt. However, it was negligible for log ratio transformation data compared with the original skew of clay (0.4). The kurtosis of all log ratio approaches ~~was-were~~ much higher compared with the consequences generated from original (untransformed) data. In terms of the k-s test ($p < 0.05$), although the p values of the original (untransformed) and different log ratio transformed data were not significant ~~and all histograms were not subject to normal distribution~~, log ratios made the ~~images of the~~ data more symmetric (~~Fig.~~according to the skews (Table 2)).



FigureTable 2. Descriptive statistical analysis for the original (untransformed) and logratio transformed soil sampling data. Note that the means generated from log ratio transformed data were back-transformed to the real space.

<u>Components</u>	<u>SD</u>	<u>CV</u>	<u>Mean</u>	<u>Median Center</u>	<u>MAD</u>	<u>Min</u>	<u>Max</u>	<u>Skew</u>	<u>Kurtosis</u>	<u>p</u>
<u>Sand</u>	<u>21.96</u>	<u>1.40</u>	<u>30.64</u>	<u>26.06</u>	<u>17.49</u>	<u>0.98</u>	<u>99.66</u>	<u>1.24</u>	<u>1.05</u>	<u>0.00</u>
<u>Silt</u>	<u>18.76</u>	<u>2.97</u>	<u>55.79</u>	<u>59.51</u>	<u>13.72</u>	<u>0.17</u>	<u>95.87</u>	<u>-0.93</u>	<u>0.82</u>	<u>0.00</u>
<u>Clay</u>	<u>9.22</u>	<u>1.47</u>	<u>13.57</u>	<u>14.43</u>	<u>10.51</u>	<u>0.03</u>	<u>39.77</u>	<u>0.40</u>	<u>-0.51</u>	<u>0.00</u>
<u>ALR Sand</u>	<u>1.69</u>	<u>0.58</u>	<u>28.69</u>		<u>1.54</u>	<u>-3.54</u>	<u>7.87</u>	<u>0.77</u>	<u>1.19</u>	<u>0.00</u>
<u>ALR Silt</u>	<u>1.13</u>	<u>1.52</u>	<u>60.54</u>		<u>0.59</u>	<u>-1.64</u>	<u>6.30</u>	<u>1.29</u>	<u>1.66</u>	<u>0.00</u>
<u>ALR Clay</u>	<u>1.31</u>	<u>0.57</u>	<u>10.78</u>		<u>0.93</u>	<u>-6.37</u>	<u>4.20</u>	<u>-1.20</u>	<u>3.66</u>	<u>0.00</u>
<u>CLR Sand</u>	<u>0.93</u>	<u>0.08</u>	<u>28.69</u>		<u>0.81</u>	<u>-2.58</u>	<u>4.25</u>	<u>0.88</u>	<u>2.11</u>	<u>0.00</u>
<u>CLR Silt</u>	<u>0.59</u>	<u>1.40</u>	<u>60.54</u>	<u>—</u>	<u>0.43</u>	<u>-2.12</u>	<u>2.70</u>	<u>-0.40</u>	<u>3.02</u>	<u>0.00</u>
<u>CLR Clay</u>	<u>0.85</u>	<u>-1.06</u>	<u>10.78</u>		<u>0.69</u>	<u>-4.64</u>	<u>0.96</u>	<u>-0.99</u>	<u>1.12</u>	<u>0.00</u>
<u>ILR Sand</u>	<u>0.92</u>	<u>0.57</u>	<u>28.69</u>		<u>0.66</u>	<u>-4.51</u>	<u>2.97</u>	<u>-1.20</u>	<u>3.66</u>	<u>0.00</u>
<u>ILR Silt</u>	<u>1.05</u>	<u>-1.06</u>	<u>60.54</u>		<u>0.85</u>	<u>-5.68</u>	<u>1.18</u>	<u>-0.99</u>	<u>1.12</u>	<u>0.00</u>
<u>ILR Clay</u>	<u>0.80</u>	<u>-1.53</u>	<u>10.78</u>		<u>0.41</u>	<u>-4.46</u>	<u>1.16</u>	<u>-1.29</u>	<u>1.66</u>	<u>0.00</u>

SD is standard deviation, CV is the coefficient of variation, and the Median Center is multivariate median based on depth measures.

5 3.2 Comparison of the machine learning models in the classification of soil texture types

3.2.1 Comparison of the validation indicators for soil texture classification

The overall accuracy of each model ranged from 0.610 to 0.647 (Fig. 3a2a). SVM had the highest overall accuracy (0.647) among the five models, followed closely by the accuracy of KNN (0.631) and RF (0.629). XGB (0.611) and MLP (0.610) were relatively lower among these models. The highest kappa coefficient was generated from XGB (0.240), followed by RF (0.238), KNN (0.234) and MLP (0.230), and the worst performer was SVM, with kappa coefficient dropping to 0.186 (Fig. 3b). With respect to the uncertainties of models with confusion indices (COIs), RF (0.49) delivered the best performance, followed by KNN (0.50), SVM (0.54) and MLP (0.55); XGB (0.72) demonstrated the highest confusion of models (Table 3).

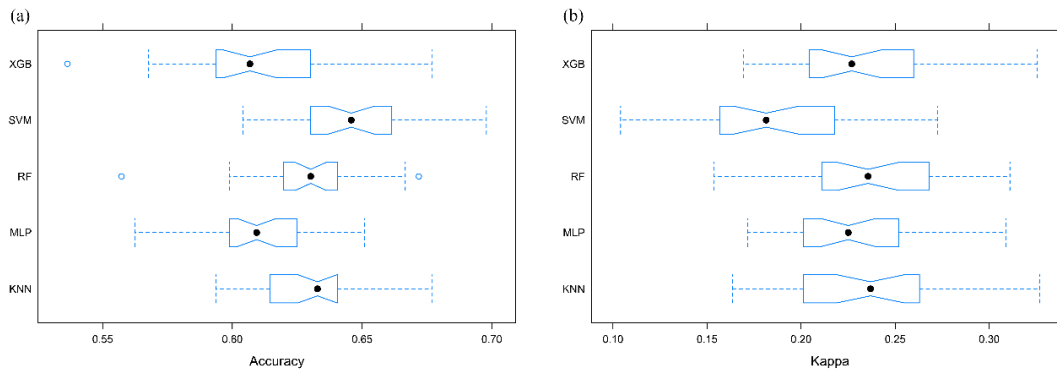


Figure 32. (a) The overall accuracies and (b) kappa coefficients for different machine-learning models of KNN, MLP, RF, SVM and XGB.

5 The AUC with regard to each soil texture type of 640 soil sampling points predicted from five different models demonstrated that the ranking of the AUC was RF>XGB>SVM>KNN>MLP in the case of fewer soil sampling points (CILo, LoSa, Sa, SaCILo and Si). However, in the case of the types with more soil sampling points (Lo, SaLo, SiLo, SiCILo), the ROC curves exhibited roughly the same shape for each model (Fig. 4); therefore, the order of performance was as follows: RF>SVM>XGB>MLP>KNN.

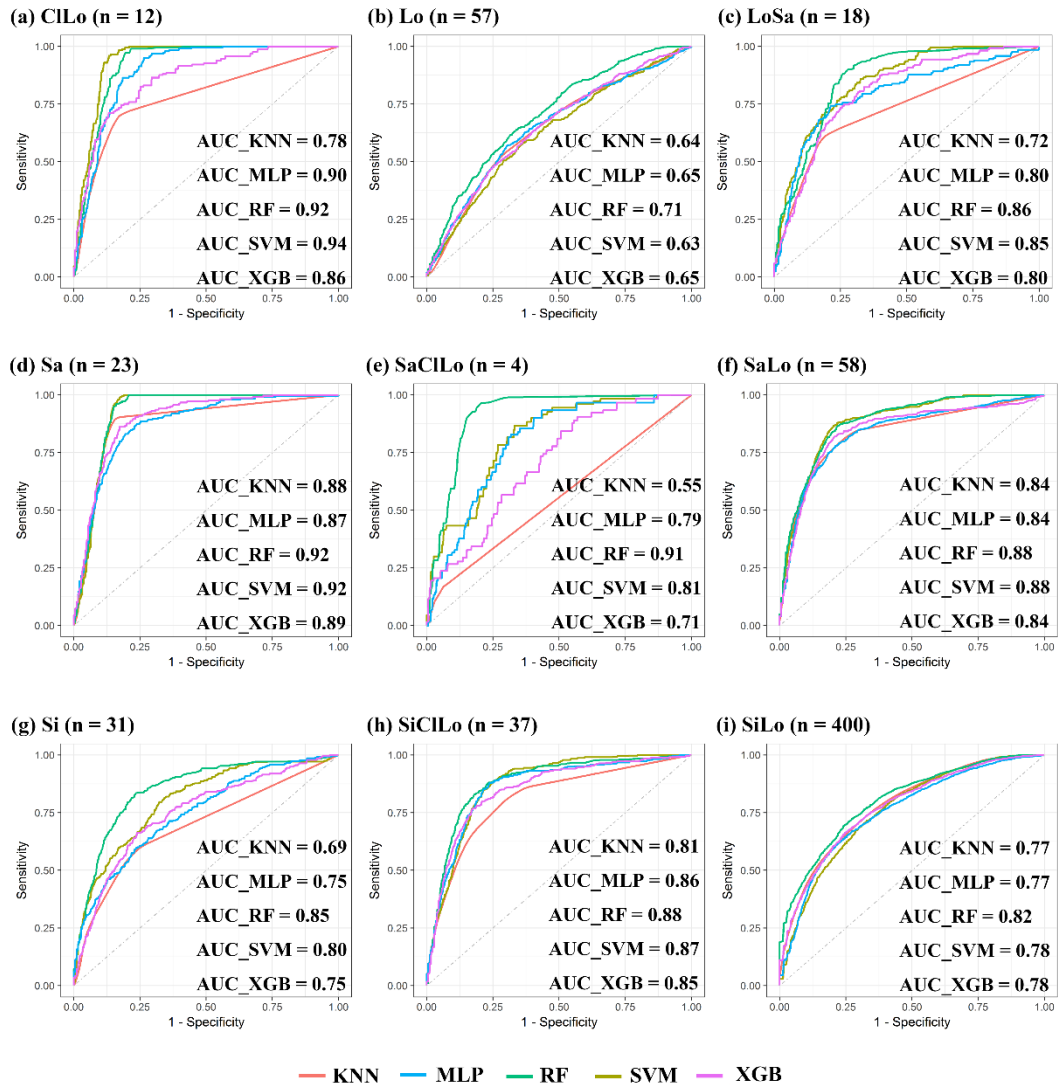


Figure 4. The AUC for different machine learning methods of each soil texture type (a) CiLo (b) Lo (c) LoSa (d) Sa (e) SaCiLo (f) SaLo (g) Si (h) SiCiLo (i) SiLo; n was the sampling points for different soil texture types.

Table 3. The comparison of COIs of different machine-learning models.

	<u>KNN</u>	<u>MLP</u>	<u>RF</u>	<u>SVM</u>	<u>XGB</u>
<u>COI</u>	<u>0.50</u>	<u>0.55</u>	<u>0.49</u>	<u>0.54</u>	<u>0.72</u>

5

We combined the PRCs with five machine-learning methods to evaluate the performance of these models with respect to predicting each soil texture type using soil psf imbalanced data with different samples of soil texture types (Fig. 53). We found that the AUPRC_s of types with fewer positive examples were typically small, especially in the case of SaCiLo (only four

5 samples), which resulted in unsatisfying consequences because the lack of soil sampling points made models learn poorly during the training process. Hence, the soil texture types (Lo, SaLo, SiLo, SiCiLo) with more positive examples delivered superior results to those with fewer positive examples. Moreover, these soil texture types had significant differences in AUPRCs. For example, SiLo, which had the largest number of samples, was the most effective among these nine types. The total AUPRC calculated by the weights of samples for AUPRC of each type was applied to evaluate the effect of each model, and the order was as follows: RF (0.646)>XGB (0.616)>KNN (0.601)>MLP (0.600)>SVM (0.599).

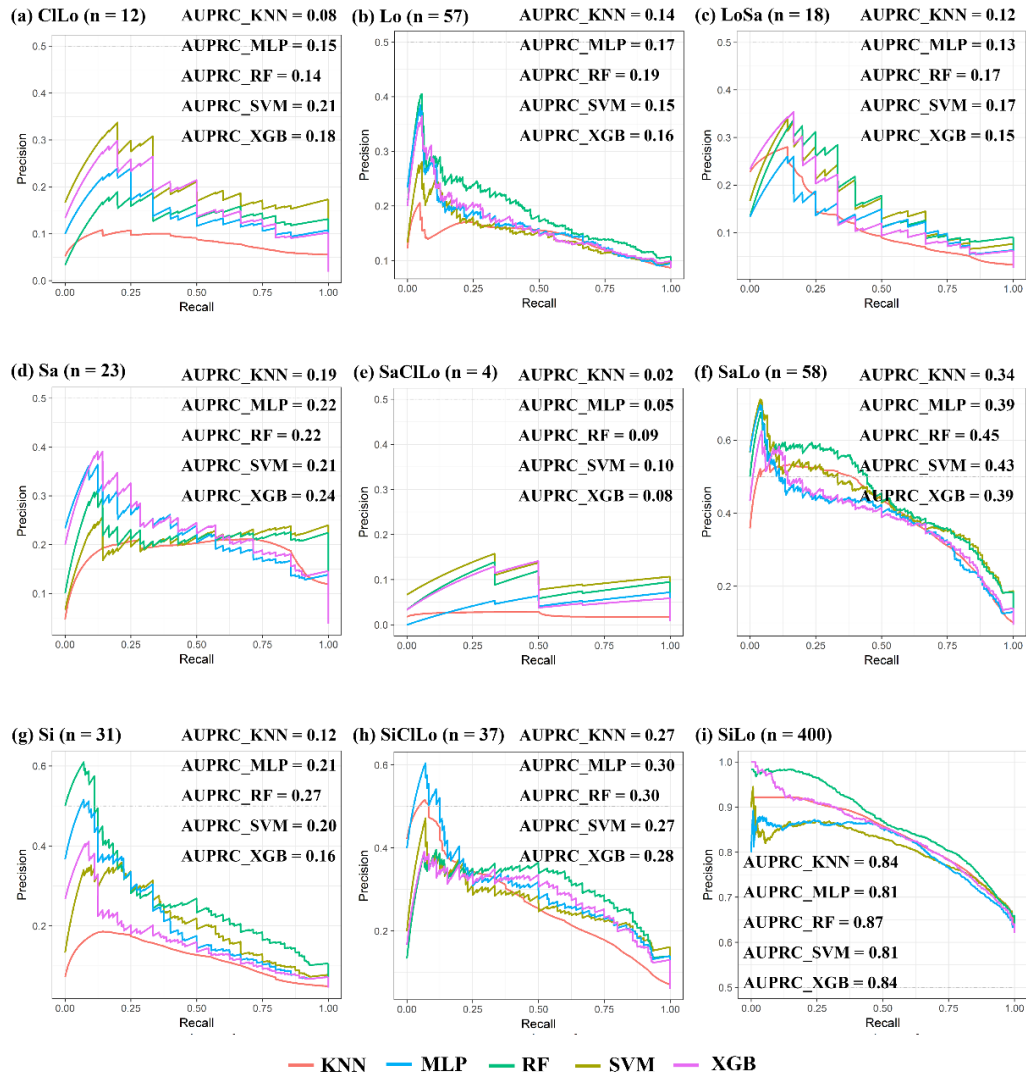


Figure 53. The AUPRC_s for different machine-learning methods of each soil texture type (a) CiLo (b) Lo (c) LoSa (d) Sa (e) SaCiLo (f) SaLo (g) Si (h) SiCiLo (i) SiLo; n was the sampling points for different soil texture types.

3.2.2 Comparison of the prediction maps for soil texture classification

Prediction maps of soil texture types in the HRB using machine-learning models delivered quite different spatial distributions in the overall performance of different models (Fig. 64). The abundance indices pointed out that all models could not predict the type of SaCILo; in other words, KNN and XGB predicted 8 of 9 types, followed closely by RF (7 of 9 types) and MLP (6 of 9 types). However, SVM predicted only two types, which was an unsatisfactory result associated with the lowest kappa coefficient (Fig. 32b). Additionally, the prediction effects of different models were different in the distributions of soil texture types in the HRB. The consequences of RF and XGB illustrated that the main soil texture types in the northwest of the lower reaches of HRB were mostly LoSa, while other prediction models produced SaLo. On the upper reaches of the HRB, soil texture types generated from RF were more abundant and more in accordance with the real environment.

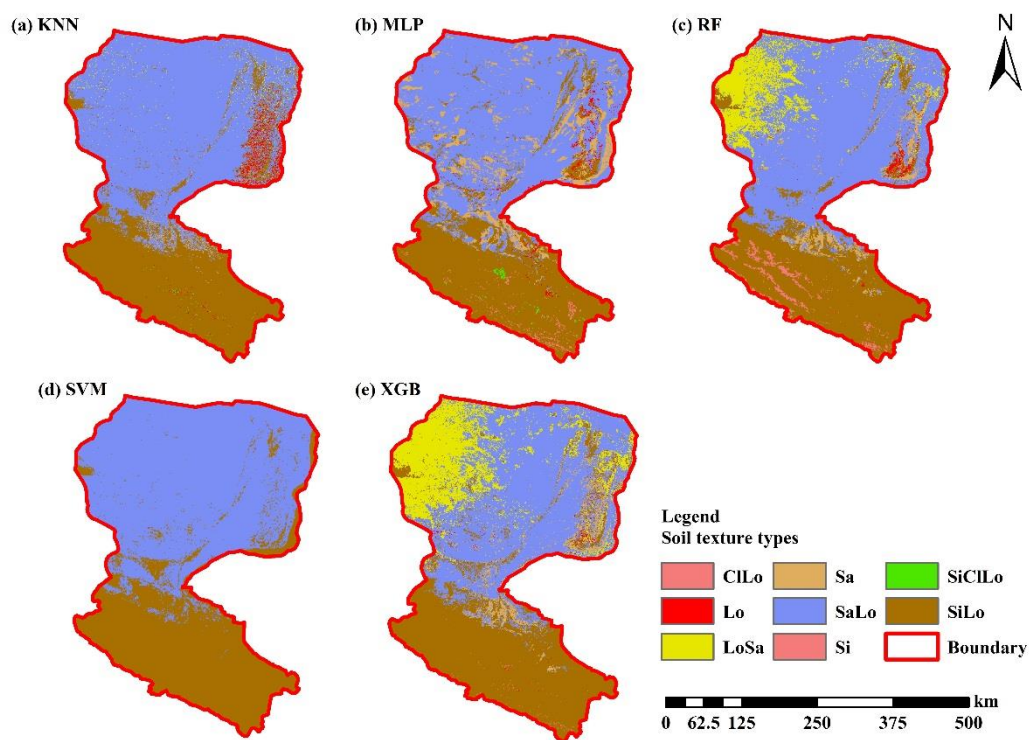


Figure 64. Soil texture classification prediction maps of different soil texture types of (a) KNN, (b) MLP, (c) RF, (d) SVM and (e) XGB.

3.3 Comparison of the machine-learning models combined with log-ratio transformed methods in the interpolation of soil psf

3.3.1 Comparison of the validation indicators and uncertainty assessment for interpolation of soil psf

We compared the performance of each machine-learning model combined with the original (untransformed) and the log ratio transformed data of soil psf. The results indicated that the accuracy of STRESS of the methods combined with log ratio transformed data were superior to other approaches using original (untransformed) data (Table 24). With respect to KNN, MLP, RF and XGB, the RMSE, MAE, R^2 and AD generated from original (untransformed) data outperformed log ratio transformed data; for SVM, log ratio transformed data delivered superior improvement. For instance, SVM_CLR and SVM_ILR had higher R^2 and lower RMSE and MAE than SVM_ORI of sand, silt and clay.

By comparison among different log ratio transformed data of the same machine-learning model, ILR and CLR outperformed ALR in these models, other than MLP, showing a slight difference. As shown in Table 24, KNN_CLR demonstrated the most remarkable performance among the three KNN models using different log ratio transformed data with highest R^2 (sand: 48.48 %; silt: 38.37 %; clay: 41.43 %) and lowest RMSE (sand: 15.82 %; silt: 14.77 %; clay: 7.09 %) and MAE (sand: 11.21 %; silt: 10.74 %; clay: 5.58 %). Furthermore, CLR and ILR generated relatively similar consequences for each model of RF and SVM; with respect to XGB, XGB_ILR showed the best performance with all indicators we measured, aside from RMSE (6.75 %) and MAE (5.36 %) of clay, and STRESS (0.63).

We also compared five different machine-learning models using the same log ratio transformation approaches. In the case of ALR, ALR_RF had the lowest RMSE (sand: 15.50 %; silt: 14.43 %; clay: 6.62 %) and MAE (sand: 10.90 %; silt: 10.52 %; clay: 5.24 %), the highest R^2 (sand: 50.57 %; silt: 41.23 %; clay: 48.90 %), and the lowest AD (0.86) and STRESS (0.61), followed by SVM_ALR, XGB_ALR, KNN_ALR and MLP_ALR. Regarding CLR and ILR, RF also produced the most preferable performance followed by SVM, XGB, KNN and MLP. For original (untransformed) data, RF outperformed other models in accordance with log ratio approaches, and the next were XGB, SVM, KNN and MLP. Therefore, it is clear that RFs demonstrated the most extraordinary indicators of RMSE, MAE, R^2 and AD from the untransformed model and the best STRESS from the log ratio models (RF_ALR, RF_CLR and RF_ILR).

For the assessments of the uncertainties of models, we calculated the standard deviation (SD) of prediction values, Table 4 showed that all machine-learning models produced low SDs of these indicators, revealing stable performance. Additionally, ORI approach delivered lower SDs than those of log ratio approaches among five machine-learning models for sand, silt and clay. For the comparison of SD of three log ratio approaches, they generated almost the same results. Moreover, the ranges of 95 % confidence interval (CI) of indicators were also computed (Table 5), which indicated relatively low values compared with assessment indicators. For KNN, MLP and RF, the ORI approach showed lower values of CI of RMSE, MAE and R^2 than those of log ratio approaches, and for SVM and XGB, SVM_CLR and XGB_CLR revealed slight better performance compared with ORI for sand (CI_RMSE: 0.49 %; CI_MAE: 0.33 %) and silt (CI_MAE: 0.44 %), respectively. For the values of the

ranges of 95 % CI of AD and STRESS, all models generated the same results (AD: 0.03, STRESS: 0.01) aside from RF ILR (AD: 0.02), showing better performance. Thus, the estimators' variabilities had reasonable order of magnitudes for the values of the estimates and these indicators were representative of the actual errors on independent test sets.

Table 4. The comparisons of accuracy of different machine-learning models combined with original (untransformed) and transformed data.

	SD			RMSE (%)			MAE (%)			R ² (%)			AD	STRESS
	Sand	Silt	Clay	Sand	Silt	Clay	Sand	Silt	Clay	Sand	Silt	Clay		
<u>KNN ALR</u>	<u>0.18</u>	<u>0.14</u>	<u>0.08</u>	<u>16.05</u>	<u>15.04</u>	<u>7.12</u>	<u>11.35</u>	<u>10.93</u>	<u>5.59</u>	<u>47.02</u>	<u>36.11</u>	<u>41.07</u>	<u>0.90</u>	<u>0.62</u>
<u>KNN CLR</u>	<u>0.18</u>	<u>0.14</u>	<u>0.08</u>	<u>15.82</u>	<u>14.77</u>	<u>7.09</u>	<u>11.21</u>	<u>10.74</u>	<u>5.58</u>	<u>48.48</u>	<u>38.37</u>	<u>41.43</u>	<u>0.88</u>	<u>0.62</u>
<u>KNN ILR</u>	<u>0.18</u>	<u>0.14</u>	<u>0.08</u>	<u>15.82</u>	<u>14.82</u>	<u>7.14</u>	<u>11.22</u>	<u>10.84</u>	<u>5.60</u>	<u>48.46</u>	<u>37.88</u>	<u>40.74</u>	<u>0.88</u>	<u>0.64</u>
<u>KNN ORI</u>	<u>0.15</u>	<u>0.11</u>	<u>0.07</u>	<u>15.51</u>	<u>14.47</u>	<u>7.05</u>	<u>11.12</u>	<u>10.51</u>	<u>5.49</u>	<u>50.59</u>	<u>40.92</u>	<u>42.24</u>	<u>0.84</u>	<u>0.66</u>
<u>MLP ALR</u>	<u>0.17</u>	<u>0.13</u>	<u>0.06</u>	<u>15.83</u>	<u>15.07</u>	<u>7.43</u>	<u>11.42</u>	<u>11.06</u>	<u>5.97</u>	<u>48.50</u>	<u>35.82</u>	<u>35.79</u>	<u>0.92</u>	<u>0.66</u>
<u>MLP CLR</u>	<u>0.16</u>	<u>0.13</u>	<u>0.06</u>	<u>15.84</u>	<u>15.07</u>	<u>7.41</u>	<u>11.45</u>	<u>11.05</u>	<u>5.96</u>	<u>48.42</u>	<u>35.86</u>	<u>36.19</u>	<u>0.92</u>	<u>0.66</u>
<u>MLP ILR</u>	<u>0.16</u>	<u>0.13</u>	<u>0.06</u>	<u>15.84</u>	<u>15.07</u>	<u>7.40</u>	<u>11.46</u>	<u>11.04</u>	<u>5.95</u>	<u>48.40</u>	<u>35.85</u>	<u>36.32</u>	<u>0.92</u>	<u>0.66</u>
<u>MLP ORI</u>	<u>0.15</u>	<u>0.11</u>	<u>0.06</u>	<u>15.80</u>	<u>14.72</u>	<u>6.96</u>	<u>11.50</u>	<u>10.85</u>	<u>5.52</u>	<u>48.75</u>	<u>38.84</u>	<u>43.72</u>	<u>0.90</u>	<u>0.68</u>
<u>RF ALR</u>	<u>0.18</u>	<u>0.15</u>	<u>0.08</u>	<u>15.50</u>	<u>14.43</u>	<u>6.62</u>	<u>10.90</u>	<u>10.52</u>	<u>5.24</u>	<u>50.57</u>	<u>41.23</u>	<u>48.90</u>	<u>0.86</u>	<u>0.61</u>
<u>RF CLR</u>	<u>0.18</u>	<u>0.15</u>	<u>0.07</u>	<u>15.28</u>	<u>14.22</u>	<u>6.61</u>	<u>10.70</u>	<u>10.25</u>	<u>5.21</u>	<u>51.95</u>	<u>42.89</u>	<u>49.16</u>	<u>0.86</u>	<u>0.61</u>
<u>RF ILR</u>	<u>0.18</u>	<u>0.15</u>	<u>0.08</u>	<u>15.27</u>	<u>14.25</u>	<u>6.66</u>	<u>10.66</u>	<u>10.26</u>	<u>5.26</u>	<u>51.99</u>	<u>42.60</u>	<u>48.28</u>	<u>0.86</u>	<u>0.61</u>
<u>RF ORI</u>	<u>0.15</u>	<u>0.12</u>	<u>0.07</u>	<u>15.09</u>	<u>13.86</u>	<u>6.31</u>	<u>10.65</u>	<u>9.99</u>	<u>5.00</u>	<u>53.28</u>	<u>45.77</u>	<u>53.75</u>	<u>0.84</u>	<u>0.66</u>
<u>SVM ALR</u>	<u>0.17</u>	<u>0.12</u>	<u>0.06</u>	<u>15.66</u>	<u>14.59</u>	<u>6.76</u>	<u>11.66</u>	<u>10.88</u>	<u>5.34</u>	<u>49.61</u>	<u>39.87</u>	<u>46.89</u>	<u>0.88</u>	<u>0.66</u>
<u>SVM CLR</u>	<u>0.16</u>	<u>0.12</u>	<u>0.06</u>	<u>15.27</u>	<u>14.36</u>	<u>6.87</u>	<u>11.01</u>	<u>10.41</u>	<u>5.41</u>	<u>52.12</u>	<u>41.85</u>	<u>45.14</u>	<u>0.87</u>	<u>0.65</u>
<u>SVM ILR</u>	<u>0.16</u>	<u>0.12</u>	<u>0.06</u>	<u>15.29</u>	<u>14.37</u>	<u>6.84</u>	<u>10.92</u>	<u>10.43</u>	<u>5.42</u>	<u>51.99</u>	<u>41.69</u>	<u>45.58</u>	<u>0.87</u>	<u>0.65</u>
<u>SVM ORI</u>	<u>0.15</u>	<u>0.11</u>	<u>0.06</u>	<u>15.30</u>	<u>14.38</u>	<u>6.92</u>	<u>10.94</u>	<u>10.32</u>	<u>5.43</u>	<u>51.98</u>	<u>41.71</u>	<u>44.45</u>	<u>0.87</u>	<u>0.67</u>
<u>XGB ALR</u>	<u>0.17</u>	<u>0.14</u>	<u>0.07</u>	<u>15.82</u>	<u>14.92</u>	<u>6.72</u>	<u>11.32</u>	<u>11.01</u>	<u>5.35</u>	<u>48.57</u>	<u>37.23</u>	<u>47.44</u>	<u>0.88</u>	<u>0.64</u>
<u>XGB CLR</u>	<u>0.19</u>	<u>0.15</u>	<u>0.07</u>	<u>15.70</u>	<u>14.80</u>	<u>6.75</u>	<u>10.96</u>	<u>10.67</u>	<u>5.39</u>	<u>49.23</u>	<u>38.10</u>	<u>46.90</u>	<u>0.88</u>	<u>0.62</u>
<u>XGB ILR</u>	<u>0.17</u>	<u>0.13</u>	<u>0.08</u>	<u>15.45</u>	<u>14.57</u>	<u>6.75</u>	<u>10.91</u>	<u>10.52</u>	<u>5.36</u>	<u>50.88</u>	<u>40.01</u>	<u>47.01</u>	<u>0.88</u>	<u>0.63</u>
<u>XGB ORI</u>	<u>0.16</u>	<u>0.12</u>	<u>0.06</u>	<u>15.15</u>	<u>14.05</u>	<u>6.47</u>	<u>10.88</u>	<u>10.15</u>	<u>5.15</u>	<u>52.85</u>	<u>44.27</u>	<u>51.36</u>	<u>0.86</u>	<u>0.68</u>

Table 5. The ranges of 95 % confidence interval (CI) of indicators for different machine-learning models combined with original (untransformed) and transformed data.

	CI RMSE (%)			CI MAE (%)			CI R ² (%)			CI AD	CI STRESS
	Sand	Silt	Clay	Sand	Silt	Clay	Sand	Silt	Clay		
<u>KNN ALR</u>	<u>0.71</u>	<u>0.65</u>	<u>0.25</u>	<u>0.51</u>	<u>0.44</u>	<u>0.16</u>	<u>4.45</u>	<u>5.03</u>	<u>4.18</u>	<u>0.03</u>	<u>0.01</u>
<u>KNN CLR</u>	<u>0.71</u>	<u>0.64</u>	<u>0.26</u>	<u>0.47</u>	<u>0.41</u>	<u>0.16</u>	<u>4.57</u>	<u>4.95</u>	<u>4.23</u>	<u>0.03</u>	<u>0.01</u>
<u>KNN ILR</u>	<u>0.73</u>	<u>0.64</u>	<u>0.27</u>	<u>0.48</u>	<u>0.41</u>	<u>0.16</u>	<u>4.78</u>	<u>5.18</u>	<u>4.40</u>	<u>0.03</u>	<u>0.01</u>
<u>KNN ORI</u>	<u>0.55</u>	<u>0.51</u>	<u>0.28</u>	<u>0.38</u>	<u>0.37</u>	<u>0.19</u>	<u>3.41</u>	<u>3.48</u>	<u>4.00</u>	<u>0.03</u>	<u>0.01</u>
<u>MLP ALR</u>	<u>0.65</u>	<u>0.67</u>	<u>0.33</u>	<u>0.38</u>	<u>0.41</u>	<u>0.20</u>	<u>4.21</u>	<u>5.07</u>	<u>5.44</u>	<u>0.03</u>	<u>0.01</u>
<u>MLP CLR</u>	<u>0.64</u>	<u>0.65</u>	<u>0.32</u>	<u>0.38</u>	<u>0.41</u>	<u>0.19</u>	<u>4.07</u>	<u>4.96</u>	<u>5.12</u>	<u>0.03</u>	<u>0.01</u>
<u>MLP ILR</u>	<u>0.64</u>	<u>0.65</u>	<u>0.32</u>	<u>0.37</u>	<u>0.41</u>	<u>0.20</u>	<u>4.04</u>	<u>4.95</u>	<u>5.04</u>	<u>0.03</u>	<u>0.01</u>
<u>MLP ORI</u>	<u>0.65</u>	<u>0.58</u>	<u>0.23</u>	<u>0.37</u>	<u>0.40</u>	<u>0.17</u>	<u>3.72</u>	<u>4.02</u>	<u>2.72</u>	<u>0.03</u>	<u>0.01</u>
<u>RF ALR</u>	<u>0.62</u>	<u>0.54</u>	<u>0.25</u>	<u>0.42</u>	<u>0.38</u>	<u>0.17</u>	<u>4.03</u>	<u>3.91</u>	<u>4.03</u>	<u>0.03</u>	<u>0.01</u>
<u>RF CLR</u>	<u>0.66</u>	<u>0.64</u>	<u>0.27</u>	<u>0.42</u>	<u>0.42</u>	<u>0.18</u>	<u>4.25</u>	<u>4.45</u>	<u>4.12</u>	<u>0.03</u>	<u>0.01</u>
<u>RF ILR</u>	<u>0.69</u>	<u>0.66</u>	<u>0.27</u>	<u>0.44</u>	<u>0.42</u>	<u>0.18</u>	<u>4.34</u>	<u>4.75</u>	<u>4.31</u>	<u>0.02</u>	<u>0.01</u>
<u>RF ORI</u>	<u>0.53</u>	<u>0.54</u>	<u>0.25</u>	<u>0.40</u>	<u>0.41</u>	<u>0.16</u>	<u>2.95</u>	<u>3.47</u>	<u>3.06</u>	<u>0.03</u>	<u>0.01</u>
<u>SVM ALR</u>	<u>0.45</u>	<u>0.49</u>	<u>0.25</u>	<u>0.35</u>	<u>0.43</u>	<u>0.17</u>	<u>3.27</u>	<u>3.74</u>	<u>2.82</u>	<u>0.03</u>	<u>0.01</u>
<u>SVM CLR</u>	<u>0.49</u>	<u>0.50</u>	<u>0.27</u>	<u>0.33</u>	<u>0.35</u>	<u>0.18</u>	<u>3.05</u>	<u>3.35</u>	<u>3.47</u>	<u>0.03</u>	<u>0.01</u>
<u>SVM ILR</u>	<u>0.51</u>	<u>0.51</u>	<u>0.25</u>	<u>0.34</u>	<u>0.36</u>	<u>0.18</u>	<u>3.07</u>	<u>3.38</u>	<u>3.18</u>	<u>0.03</u>	<u>0.01</u>
<u>SVM ORI</u>	<u>0.51</u>	<u>0.49</u>	<u>0.25</u>	<u>0.34</u>	<u>0.35</u>	<u>0.17</u>	<u>2.92</u>	<u>3.14</u>	<u>2.95</u>	<u>0.03</u>	<u>0.01</u>
<u>XGB ALR</u>	<u>0.67</u>	<u>0.57</u>	<u>0.23</u>	<u>0.48</u>	<u>0.41</u>	<u>0.16</u>	<u>4.07</u>	<u>3.97</u>	<u>3.60</u>	<u>0.03</u>	<u>0.01</u>
<u>XGB CLR</u>	<u>0.73</u>	<u>0.65</u>	<u>0.25</u>	<u>0.44</u>	<u>0.44</u>	<u>0.16</u>	<u>4.90</u>	<u>5.00</u>	<u>3.82</u>	<u>0.03</u>	<u>0.01</u>
<u>XGB ILR</u>	<u>0.72</u>	<u>0.69</u>	<u>0.26</u>	<u>0.46</u>	<u>0.48</u>	<u>0.19</u>	<u>4.52</u>	<u>4.86</u>	<u>4.44</u>	<u>0.03</u>	<u>0.01</u>
<u>XGB ORI</u>	<u>0.60</u>	<u>0.61</u>	<u>0.24</u>	<u>0.41</u>	<u>0.46</u>	<u>0.16</u>	<u>3.40</u>	<u>4.03</u>	<u>2.90</u>	<u>0.03</u>	<u>0.01</u>

3.3.2 Comparison of the interpolation maps of soil psf

- 5 Interpolation maps of soil psf (sand, silt and clay) using log ratio transformed data (ILR) and original (untransformed) data were represented in Figs. 75, S1 and S2. At first glance, there was a negligible difference between ILR and ORI based on the same machine-learning model. However, the maps generated from models combined with ILR transformed data showed closer ranges to the original soil sampling data in the case of sand (0.98-99.66 %), silt (0.17-95.87 %) and clay (0.03-39.77 %), and the texture features were more suitable for the distributions of the real environment (Figs. 75, S1 and S2). With respect to
- 10 different machine-learning models, RF and XGB delivered more detailed information about texture features in prediction maps than did KNN, SVM and MLP.

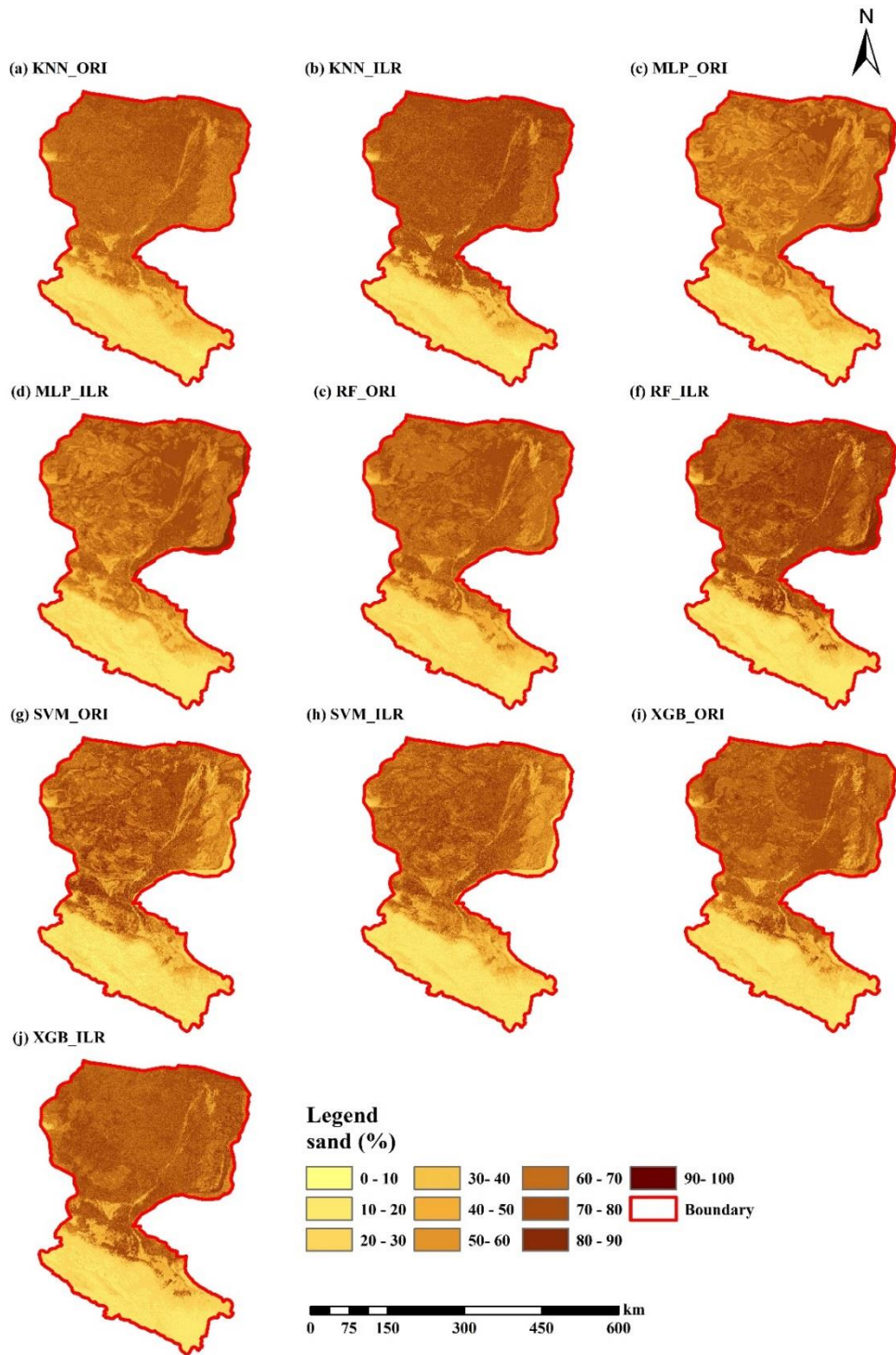


Figure 75. The interpolation maps of sand fraction.

3.4 Comparison of direct and indirect soil texture classification

3.4.1 Comparison of the validation indicators for direct and indirect soil texture classification

Compared with the classification performance of the five machine-learning models using original (untransformed) data, the overall ~~accuracy~~ accuracy and kappa coefficients of models ~~combined~~ using log ratio transformed data were improved, especially RF and XGB, which combined with all three log ratio approaches were superior to the interpolation methods using original data. Table ~~36~~ ~~shows~~ ~~showed~~ that the overall accuracy (0.631) and kappa coefficient (0.245) of the original method in KNN models were better than any other log ratio transformed methods. In summary, the ILR transformation method of five machine-learning models showed the highest overall accuracy among three log ratio transformation approaches (KNN: 0.628; MLP: 0.614; RF: 0.631; SVM: 0.631; XGB: 0.632), which also demonstrated the best performance with regard to kappa coefficients (KNN: 0.244; RF: 0.291; SVM: 0.239; XGB: 0.252), except for MLP (ALR: 0.216; CLR: 0.216; ILR: 0.214). We also compared direct classification (Fig. ~~32~~) with indirect classification and found that the highest values of overall accuracy of indirect classification (KNN: 0.631; MLP: 0.614; RF: 0.628; SVM: 0.638; XGB: 0.632) were slightly decreased in comparison of direct classification (KNN: 0.631; MLP: 0.610; RF: 0.629; SVM: 0.647; XGB: 0.611) for RF and SVM, and improved or kept stable for MLP and XGB, and KNN, respectively. In turn, the kappa coefficients were greatly modified using indirect classification (KNN: 0.245; MLP: 0.216; RF: 0.291; SVM: 0.239; XGB: 0.252) compared with direct classification (KNN: 0.234; MLP: 0.230; RF: 0.238; SVM: 0.186; XGB: 0.240), other than MLP; peculiarly, RF_ILR increased the kappa coefficient to 0.291 (21.3 % improvement) while keeping accuracy stable, ~~which showed~~ ~~showing~~ the highest kappa coefficient among these methods.

Table 36. Overall ~~accuracy~~ accuracy and kappa coefficients calculated from soil texture classification by the interpolated maps from five models using original (untransformed) data and log ratio transformed data.

Methods	Overall accuracy	Kappa coefficient
KNN_ALR	0.623	0.236
KNN_CLR	0.627	0.241
KNN_ILR	0.628	0.244
KNN_ORI	0.631	0.245
MLP_ALR	0.614	0.216
MLP_CLR	0.614	0.216
MLP_ILR	0.614	0.214
MLP_ORI	0.611	0.216
RF_ALR	0.619	0.284
RF_CLR	0.625	0.276
RF_ILR	0.628	0.291

RF_ORI	0.619	0.279
SVM_ALR	0.591	0.205
SVM_CLR	0.630	0.227
SVM_ILR	0.631	0.239
SVM_ORI	0.638	0.232
XGB_ALR	0.610	0.226
XGB_CLR	0.612	0.240
XGB_ILR	0.632	0.252
XGB_ORI	0.619	0.239

3.4.2 The prediction performance of soil texture types from different methods

The distributions of soil texture classes using original (untransformed) data and ILR transformed data ~~are~~ were illustrated in the USDA soil texture triangle (Fig. 86). The triangle of the original data (Fig. 86a) ~~shows~~ demonstrated wider ranges of spatial dispersion than the interpolation data using machine-learning models, revealing the properties of aggregate from the sides to the center of triangles. With respect to these machine-learning models, RF showed the most dispersed feature in accordance with the original data. The distributions predicted from models combined with ILR transformed data were more discrete and more associated with the original soil psf data than those resulting from ORI approaches. The results of prediction represented striking differences in that the error ratio (red color) of soil sampling points on types of LoSa, SaLo and Lo (left side of triangles) were significantly more than those on types of SiLo and Si (the right side of triangles) for most models, especially KNN and MLP. The log ratio approaches overestimated the content of silt in the process of transformation (Fig. Table 2); in this way, these points were biased to the right of the USDA soil texture triangle based on overall contraction (regression smoothing effects), crossing the classification boundary and becoming other soil texture types. RF_ILR (Fig. 86f) delivered the highest right ratio (RR) among these models, and the classification accuracy was enhanced using the ILR approach (83.9%) compared with the ORI approach (81.7%). In the case of other models, the differences between original and log ratio approaches were negligible. We also compared the RR_s of indirect classification models with those of direct classification, demonstrating all RR_s of direct classification were higher (KNN: 67.97 %; MLP: 75.16 %; RF: 100 %; SVM: 66.09 %; XGB: 81.09 %), especially RF and XGB; however, we removed this evaluation indicator because the same data sets were employed in the processes of training and predicting.

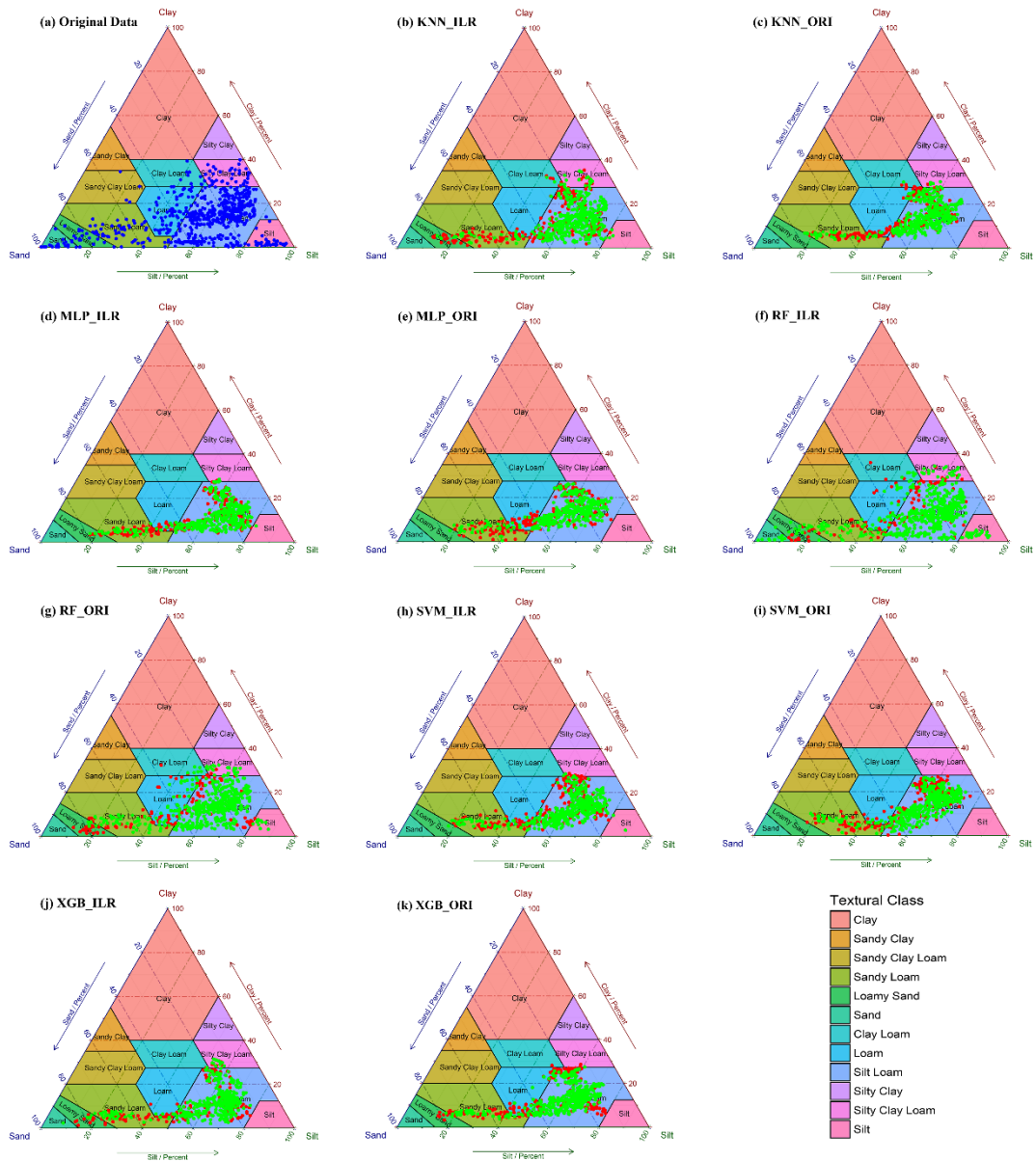


Figure 86. Soil texture types of 640 soil samples shown in [the](#) USDA texture triangle. The results of soil psf were generated from (a) original (untransformed) data, (b) KNN_ILR (65.0 %), (c) KNN_ORI (65.9 %), (d) MLP_ILR (63.3 %), (e) MLP_ORI (63.6 %), (f) RF_ILR (83.9 %), (g) RF_ORI (81.7 %), (h) SVM_ILR (66.1 %), (i) SVM_ORI (66.4 %), (j) XGB_ILR (67.8 %), and (k) XGB_ORI (68.0 %). Note that the predicted right-ratios (RRs) of the soil texture types were in the bracket after interpolators.

3.4.3 Comparison of prediction maps of direct and indirect soil texture classification

Fig. 97 ~~shows~~indicated the ~~similarity~~similarities of the three log₋ratio transformation methods. The soil texture maps predicted using original data ~~is~~were different from those generated ~~by~~from log₋ratio transformed data, and the classification maps from the machine₋learning models combined with the log₋ratio transformed data had more detailed information. Three

5 log₋ratio transformation methods of the same machine₋learning model ~~are~~were similar in the number of each type predicted; however, there ~~are~~were some differences between methods using original data and those using log₋ratio transformed data. All machine₋learning models combined with original data predicted more types of Lo and SaLo, and ~~less~~fewer types of LoSa and Si, which could also be presented in Fig. 97. The performance of different machine₋learning models, especially ~~in~~on the lower reaches of the Heihe River Basin, ~~was~~were also compared, for log₋ratio transformation methods, ~~for~~in KNN, KNN_ALR,

10 and KNN_CLR predicted more type of LoSa than KNN_ILR in the north of lower reaches; for each model of MLP and RF, the differences were slight; more types of Lo in the northwest of lower reaches and less LoSa near the Heihe River were generated by SVM_ALR, compared with SVM_CLR and SVM_ILR; for XGB, the performance of three maps were different due to the prediction of LoSa. We also compared the prediction of the soil texture types by direct classification (Fig. 64) with those generated ~~by~~from indirect classification using the same machine₋learning model, ~~and found~~revealing completely

15 difference between them on the lower reaches of Heihe River Basin; such as the distribution of LoSa; on the middle and upper reaches of Heihe River Basin, all the prediction maps were similar, mainly distributed with SiLo.

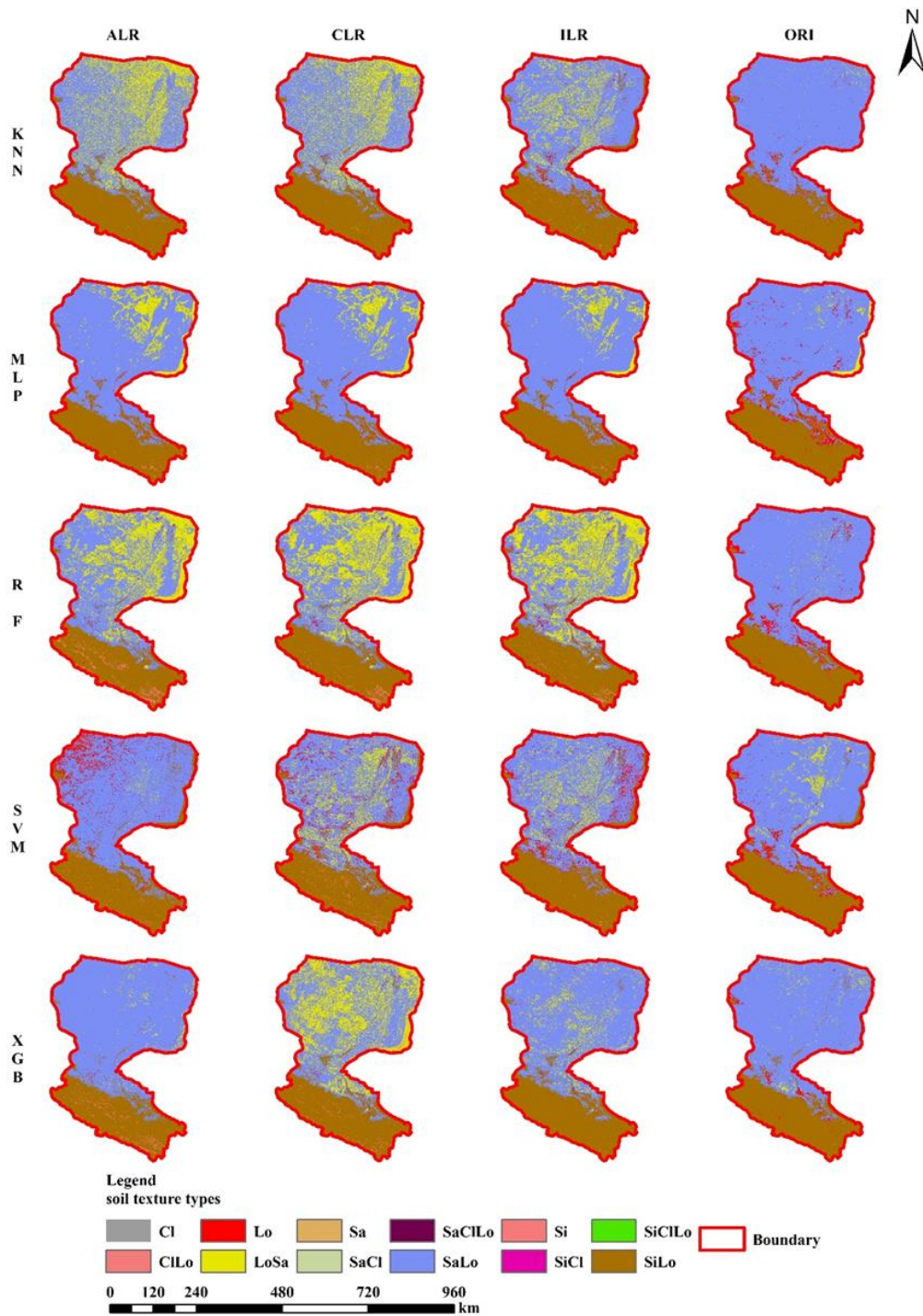


Figure 97. Soil texture classification prediction maps by soil psf interpolation (ALR, CLR, ILR log₋ratio transformation methods and the original method) of KNN, MLP, RF, SVM and XGB.

3.4.4 Comparison of time-spending for each model in soil texture classification and soil psf interpolation

Time spending for models was computed to compare the efficiency of different machine-learning models in soil texture classification and soil psf interpolation (Fig. 108). Because the differences in time ~~spendingspent~~ among ORI and log ratio approaches were similar, time spent of ILR was selected for soil psf interpolation. For the different models, RFs required the longest time for both classification (453.73 s) and regression (188.87 s), which may cause it to lose advantages when dealing with big data sets. KNN (classification: 4.2 s, regression: 23.6 s) and SVM (classification: 4.15 s, regression: 12.4 s) both showed shorter time in not only classification but also regression. Likewise, XGB (classification: 21.6 s, regression: 17.13 s) was much more stable and used less time, and the data processes were simpler compared with MLP (classification: 47.28 s, regression: 152.31 s). Moreover, ~~it-XGB~~ delivered better performance than KNN and SVM in prediction maps of HRB, demonstrating an effective way of dealing with larger data.

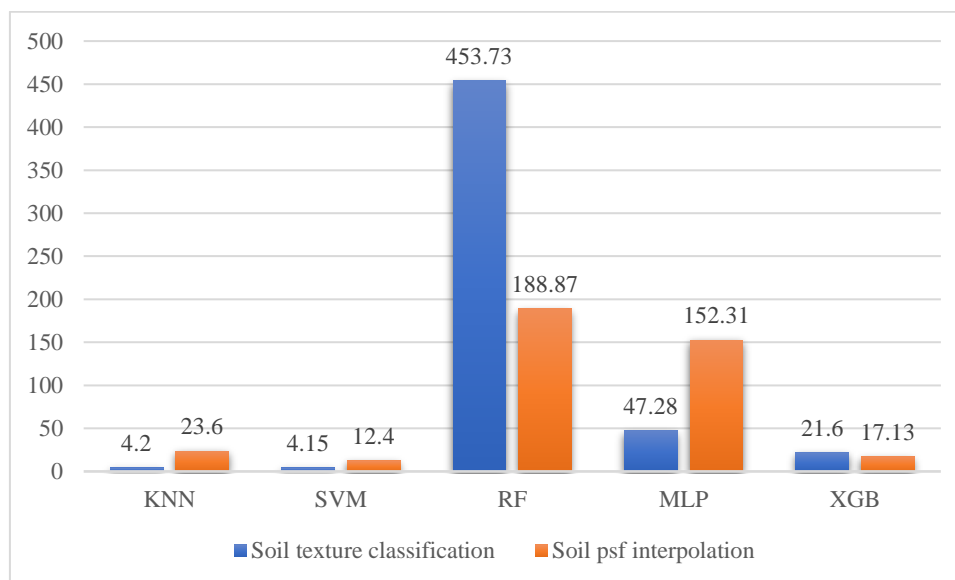


Figure 108. Average time spent running 30 times ~~for-of~~ KNN, MLP, RF, SVM and XGB of soil texture classification and soil psf interpolation.

4 Discussion

4.1 The systematic comparison of the five machine learning models

As mentioned previously, we compared the performance of different machine-learning methods containing KNN, MLP, RF, SVM and XGB. The results ~~demonstrate-demonstrated~~ that SVM had the highest overall accuracy and XGB generated the highest kappa coefficient with respect to direct soil texture classification; considering the comprehensive evaluation of AUC

and AUPRC, RF showed the best performance among these machine-learning models. In the case of soil psf interpolation, the indicators of RMSE, MAE, R^2 , AD and STRESS showed that RFs outperformed other machine-learning models, which also indicated additional information in prediction maps of sand, silt and clay ~~and as well as~~ models of XGB. For the ~~indirection~~ classification of soil texture, the USDA soil texture triangles generated from RF were the closest to the distribution of the original data (Fig. ~~8a6a~~), with the highest classification right ratio. Prediction maps of indirect soil texture classification were also considered, ~~demonstrating moreover~~, RF and MLP models were more suitable for the real environment, especially the models combined with log ratio transformation approaches. Time ~~spending spent~~ of different machine-learning models showed that KNN, SVM and XGB required less time than RF and MLP to fit large data sets.

The comparisons of machine-learning models were also mentioned in previous reports. Heung et al. (2016) demonstrated that tree learners, such as RFs, delivered better performance than KNN and SVM due to the advantages of the interpretability of the results for classification problems in soil science; tree learners (decision trees) were also shown by Taghizadeh-Mehrjardi et al. (2015), indicating that the decision trees and ANN outperformed KNN, RF and SVM. ANNs, however, were typically complicated, which was true for our study due to the standardization and back transformation of MLP. In contrast, Wu et al. (2018) proposed that SVM revealed reliable consequences in direct soil texture classification, which was quite different from our results. In general, as binary classifiers, multi-class tasks can be handled as well using SVM; however, this is no longer the case in our study, as only ~~2two~~ types of soil texture were generated from SVM, showing unsatisfactory results in both kappa coefficients and prediction maps. The consequences may be explained by the imbalanced data of soil texture types. For more information about tree learners in soil science for regression, Hengl et al. (2017) found lower R^2 using XGB than RF on a global-scale prediction. Zeraatpisheh et al. (2018) put forward the lowest RMSE and the highest R^2 using RF compared with multiple linear regression and regression trees for the prediction of clay, and this conclusion was similar to our study. For more general validity, soil psf sampling data and the range of study area should be taken into account. In our study, data did not follow normal distribution, even the log ratio approaches were employed, and p values were not significant in k-s test; additionally, spatial prediction of soil psf and soil texture based on machine-learning methods were applied for not only a large amount of soil sampling data but also regional scale study area. From this point of view, our consequences therefore could provide more general evidence to other researches.

4.2 The systematic comparison of the models combined with three log-ratio transformed data and original data

We compared the performance of models combined with three types of log ratio transformed data and original (untransformed) data for soil psf interpolation and indirect soil texture classification, and the results showed that the models using original data performed better in the case of indicators, such as RMSE, MAE, R^2 and AD, while the models using log ratio transformed data improved ~~the~~-STRESS. The interpolation maps of soil psf using ~~the~~-ILR approach illustrated closer ranges of soil sampling data than those based on ~~the~~ ORI approach. With respect to the indirect soil texture classification, models using log ratio transformed data improved the overall ~~aeuuaeies~~accuracy and kappa coefficients, such as RF and XGB. The USDA soil texture

triangles showed more discrete distribution and more accordance with soil sampling data using ~~the~~ ILR transformation method. Better performance was shown in soil texture classification prediction maps generated from log ratio transformed data. Among the three log ratio approaches, ILR and CLR were superior to ALR for the reason of more accurate indicators of soil psf interpolation and indirect soil texture classification, as well the performance of prediction maps. Note that ILR and CLR approaches provided approximate equivalent consequences; firstly, ILR and CLR were isometric transformation methods, which could preserve distances; ALR however was not isometric. Secondly, CLR can transform into ILR using $(D - 1) \times D$ orthogonal identity matrix (Egozcue et al. 2003), ILR and CLR are the keys of the application of correlation analysis and principal component analysis (PCA) to compositions, respectively, and ILR variables should interpret and analyze in the CLR space in some cases (Grunsky, 2010). Further, slightly better performance of ILR than CLR were demonstrated in Table 4 because ILR overcomes the data collinearity problem and sub-compositional incoherence of CLR, by using an appropriate choice of the basis with regard to the latter case (Egozcue and Pawlowsky-Glahn, 2005). Additionally, log ratio approaches modified soil sampling data to become more symmetric (Filzmoser et al., 2009); however, this improvement was not greatly effective. Fig-Table 2 illustrated that soil sampling data ~~for~~ of sand and clay were right-skewed, and silt was left-skewed because the silt component was predominant. ~~The~~ ALR transformed-transformation method enhanced soil sampling data of sand; nevertheless, ~~the~~ ALR_sand was still right-skewed, similar to ~~the~~ CLR_sand, presenting the lack of adjustment. In contrast, ~~the~~ ILR_sand changed from right-skewed to left-skewed; from this point of view, the over-adjustment was revealed. Similarly, the lack of adjustments was also shown in CLR_silt and ILR_silt; over-adjustments included ALR_silt, ALR_clay, CLR_clay and ILR_clay, making images that were different from normal distribution, and the p values of k-s tests were not significant. In our previous research (Wang and Shi, 2017), ~~the~~ ILR approach had better performance than ALR and CLR, with the highest R^2 and lowest AD. ~~The~~ CLR approach also performed well due to the lowest RMSE and mean error (ME) among the three log ratio approaches. When comparing the original (untransformed) and log ratio approaches, kriging approaches based on ~~the~~ log ratio delivered slightly decreased ~~accuracies~~ accuracy, which was similar to the conclusion in our study. Log ratio approaches can overcome the “closure effect”, spurious correlation and negative bias of compositional data, and the transformed data will be more symmetric and follow a normal distribution (Odeh et al., 2003; Wang and Shi, 2017). However, the indicators and methods on the original scale were designed in the Euclidean geometry. Thus, there has been a concern in log ratio approaches that the optimal estimate of log ratio transformed data does not deliver the optimal estimate of the compositions back-transformed to the real space, which leads to the result that the ORI approach outperformed those in log-ratio geometry.

4.3 The systematic comparison of the direct and indirect classification for soil psf

30 Indirect classification showed not only better performance with respect to accuracy evaluation but also more accordance with the real environment than direct classification. The highest kappa coefficient generated from indirect classification (RF_ILR:

0.291) demonstrated obvious improvement (approximately 21.3 %) compared with that of direct classification (XGB: 0.240), keeping the highest overall accuracy stable (-1.4 %) at the same time (direct: 0.647; indirect: 0.638, respectively).

Compared with the real soil texture distribution and environment of the HRB, SiLo overlaid the upper reaches of HRB, and SaLo and Lo were in the south of the upper reaches of HRB showed strip distribution. Moreover, an uncovered area was detected in the northwest of the lower reaches of HRB, where it cannot be predicted due to a lack of information (soil samples) input in the process of model training. The main soil texture types of the lower reaches of the HRB were SiLo, LoSa and small amounts of SaLo and Lo, which distributed in the uncovered area. The main soil texture types predicted by direct classification using machine-learning models were SaLo and SiLo; RF and XGB delivered much more LoSa than other direct classification models. However, all these models predicted that the main soil type of the lower reaches of HRB was SaLo, which was not fitted for the real environment (LoSa). In addition, because of the limitation of the train sets, direct classification can only predict types in the training data; in contrast, indirect classification broke such limitations, and new prediction types arose due to the transformation from soil psf to soil texture types. Moreover, more suitable matching performance with the real environment should be considered, such as the log ratio approaches of MLP, RF, KNN_ ALR, KNN_ ILR and XGB_ CLR. The direct soil texture classification generated relative unsatisfactory consequences. Although the indirect soil texture classification outperformed the direct one, kappa coefficients for indirect classification at fair-level (0.21-0.40) also need to be enhanced. Hence, soil sampling data appear to be comprehensively meaningful, considering accuracy improvement. In the case of soil sampling data, the laser diffraction approach we mentioned above was applied to obtain the discrete representation of particle size curves based on the given quantiles of these curves, i.e., soil particle size fractions (psf, sand, silt and clay). Subsequently, soil psf data were separately modeled for prediction and validation. Another perspective of soil psf should be considered, i.e., the probability density functions of particle size curves (so-called functional compositions), which are non-negative values that integrate to 1 (or 100 %) and can be considered as compositional data with infinitesimal parts (Menafoglio et al., 2014). Unlike conventional approaches, the viewpoints of functional compositions are beneficial to acquiring complete and continuous information rather than discrete information (sand, silt and clay) and soil texture and soil particle size fractions can be extracted using the stochastic simulation of soil particle-size curves (Menafoglio et al., 2016b). Previous studies applied such functional-compositional data for the simulation of particle size curves combined with geostatistical or machine-learning methods such as kriging and bayes approaches (Menafoglio et al., 2016a) in hydrogeology, demonstrating more remarkable results compared with traditional methods. Therefore, which data should be used is the key points of accuracy improvement in future research.

5 Conclusion

We systematically compared a total of 45 models for direct and indirect soil texture classification, and soil psf interpolation using five machine-learning approaches combined with original (untransformed) and three different log ratio transformed data in the HRB. The results ~~indicate~~ indicated that as flexible and stable models, tree learners such as RF delivered powerful

performance in both classification and regression and were superior to other machine-learning models mentioned above. As a new and sub-optimal machine-learning method in soil science, XGB appeared to be more meaningful and more computationally efficient when dealing with large data sets. In addition, the log ratio approaches had advantages of modifying STRESS in soil psf interpolation. Moreover, the indirect soil texture classification outperformed the direct one, especially when combined with the log ratio approaches. The indirect soil texture classification generated preferable consequences in both cases of accuracy indicators and prediction maps. More appropriate environmental covariates and interpolation techniques, more symmetric distribution of soil sampling data (or multiple perspectives of compositional data selection), and systematic parameter adjustment algorithms of compositional data are key to improving accuracy in the future.

10

Data availability. The soil sampling data (<http://westdc.westgis.ac.cn/DOI:10.3972/heihe.009.2013.db>; <http://westdc.westgis.ac.cn/DOI:10.3972/heihe.00135.2016.db>; <http://westdc.westgis.ac.cn/DOI:10.3972/hiwater.147.2013.db>; <http://westdc.westgis.ac.cn/DOI:10.3972/heihe.037.2014.db>; <http://westdc.westgis.ac.cn/DOI:doi:10.3972/heihe.0034.2013.db>;

15 <http://westdc.westgis.ac.cn/DOI:10.3972/heihe.093.2013.db>) and part of environmental covariates data can be accessed through <http://westdc.westgis.ac.cn/> (last access: 29 October 2018). The meteorological data can be accessed through <http://data.cma.cn/> (last access: 29 October 2018).

20 *Author contributions.* WS contributed to soil data sampling, oversaw the design of the entire project. MZ performed the analysis and wrote the manuscript. Both authors contributed to writing this paper and interpreting data.

Competing interests. The authors declare that they have no conflict of interest.

25

Acknowledgements. This study was supported by [the National Key Research and Development Program of China \(No. 2017YFA0604703\)](#), the National Natural Science Foundation of China (Grant No. 41771111 and 41771364), Fund for Excellent Young Talents in Institute of Geographic Sciences and Natural Resources Research, Chinese Academy of Sciences (2016RC201), and the Youth Innovation Promotion Association, CAS (No. 2018071).

30

References

- Abdi, D., Cade-Menun, B. J., Ziadi, N., and Parent, L.-E.: Compositional statistical analysis of soil p-31-nmr forms, *Geoderma*, 257, 40-47, <https://doi.org/10.1016/j.geoderma.2015.03.019>, 2015.
- Adhikari, K., and Hartemink, A. E.: Linking soils to ecosystem services - a global review, *Geoderma*, 262, 101-111, <https://doi.org/10.1016/j.geoderma.2015.08.009>, 2016.
- 5 Aitchison, J.: The statistical-analysis of compositional data, *Journal of the Royal Statistical Society Series B-Methodological*, 44, 139-177, 1982.
- Aitchison, J.: On criteria for measures of compositional difference, *Mathematical Geology*, 24, 365-379, <https://doi.org/10.1007/bf00891269>, 1992.
- 10 Aitchison, J.: The one-hour course in compositional data analysis or compositional data analysis is simple, 1997.
- Bagheri Bodaghabadi, M., Antonio Martinez-Casasnovas, J., Salehi, M. H., Mohammadi, J., Esfandiarpour Borujeni, I., Toomanian, N., and Gandomkar, A.: Digital soil mapping using artificial neural networks and terrain-related attributes, *Pedosphere*, 25, 580-591, [https://doi.org/10.1016/s1002-0160\(15\)30038-2](https://doi.org/10.1016/s1002-0160(15)30038-2), 2015.
- Bationo, A., Kihara, J., Vanlauwe, B., Waswa, B., and Kimetu, J.: Soil organic carbon dynamics, functions and management in west african agro-ecosystems, *Agricultural Systems*, 94, 13-25, <https://doi.org/10.1016/j.agsy.2005.08.011>, 2007.
- 15 Bedall, F. K., and Zimmermann, H.: Algorithm as 143: The mediancentre, *Journal of the Royal Statistical Society. Series C (Applied Statistics)*, 28, 325-328, 10.2307/2347218, 1979.
- Behrens, T., and Scholten, T.: Chapter 25 a comparison of data-mining techniques in predictive soil mapping, in: *Developments in soil science*, edited by: Lagacherie, P., McBratney, A. B., and Voltz, M., Elsevier, 353-617, 2006.
- 20 Bergmeir, C., and Benitez, J. M.: Neural networks in R using the stuttgart neural network simulator: RSNNS, *Journal of Statistical Software*, 46, 1-26, 2012.
- Breiman, L.: Bagging predictors, *Machine Learning*, 24, 123-140, <https://doi.org/10.1023/a:1018054314350>, 1996.
- Breiman, L.: Random forests, *Machine Learning*, 45, 5-32, <https://doi.org/10.1023/a:1010933404324>, 2001.
- Brown, D. J., Clayton, M. K., and McSweeney, K.: Potential terrain controls on soil color, texture contrast and grain-size deposition for the original catena landscape in uganda, *Geoderma*, 122, 51-72, <https://doi.org/10.1016/j.geoderma.2003.12.004>, 2004.
- 25 Brus, D. J., Kempen, B., and Heuvelink, G. B. M.: Sampling for validation of digital soil maps, *European Journal of Soil Science*, 62, 394-407, <https://doi.org/10.1111/j.1365-2389.2011.01364.x>, 2011.
- Burges, C. J. C.: A tutorial on support vector machines for pattern recognition, *Data Mining and Knowledge Discovery*, 2, 121-167, <https://doi.org/10.1023/a:1009715923555>, 1998.
- 30 Burrough, P. A., van Gaans, P. F. M., and Hootsmans, R.: Continuous classification in soil survey: Spatial correlation, confusion and boundaries, *Geoderma*, 77, 115-135, [https://doi.org/10.1016/S0016-7061\(97\)00018-9](https://doi.org/10.1016/S0016-7061(97)00018-9), 1997.

- Butler, J. C.: Effects of closure on the moments of a distribution, Journal of the International Association for Mathematical Geology, 11, 75-84, [10.1007/bf01043247](https://doi.org/10.1007/bf01043247), 1979.
- Camera, C., Zomeni, Z., Noller, J. S., Zissimos, A. M., Christoforou, I. C., and Bruggeman, A.: A high resolution map of soil types and physical properties for cyprus: A digital soil mapping optimization, *Geoderma*, 285, 35-49, <https://doi.org/10.1016/j.geoderma.2016.09.019>, 2017.
- Chen, T., and Guestrin, C.: Xgboost: A scalable tree boosting system, Proceedings of the 22nd ACM SIGKDD International Conference on Knowledge Discovery and Data Mining, San Francisco, California, USA, 2016.
- Chen, T., He, T., Benesty, M., Khotilovich, V., Tang, Y., Cho, H., Chen, K., Mitchell, R., Cano, I., Zhou, T., Li, M., Xie, J., Lin, M., Geng, Y., and Li, Y.: Xgboost: Extreme gradient boosting, R package version 0.71.2, available at: <https://CRAN.R-project.org/package=xgboost> (last access: 18 November 2018), 2018.
- Conrad, O., Bechtel, B., Bock, M., Dietrich, H., Fischer, E., Gerlitz, L., Wehberg, J., Wichmann, V., and Böhner, J.: System for automated geoscientific analyses (saga) v. 2.1.4, *Geosci. Model Dev.*, 8, 1991-2007, <https://doi.org/10.5194/gmd-8-1991-2015>, 2015.
- Cortes, C., and Vapnik, V.: Support-vector networks, *Machine Learning*, 20, 273-297, <https://doi.org/10.1023/a:1022627411411>, 1995.
- Cover, T. M., and Hart, P. E.: Nearest neighbor pattern classification, *Ieee Transactions on Information Theory*, 13, 21, <https://doi.org/10.1109/tit.1967.1053964>, 1967.
- Crouvi, O., Pelletier, J. D., and Rasmussen, C.: Predicting the thickness and aeolian fraction of soils in upland watersheds of the mojave desert, *Geoderma*, 195, 94-110, <https://doi.org/10.1016/j.geoderma.2012.11.015>, 2013.
- Davis, J., and Goadrich, M.: The relationship between precision-recall and roc curves, Proceedings of the 23rd international conference on Machine learning, Pittsburgh, Pennsylvania, USA, 2006.
- Egozcue, J. J., Pawlowsky-Glahn, V., Mateu-Figueras, G., and Barcelo-Vidal, C.: Isometric logratio transformations for compositional data analysis, *Mathematical Geology*, 35, 279-300, <https://doi.org/10.1023/a:1023818214614>, 2003.
- Egozcue, J. J., and Pawlowsky-Glahn, V.: Groups of parts and their balances in compositional data analysis, Math. Geol., 37, 795-828, [10.1007/s11004-005-7381-9](https://doi.org/10.1007/s11004-005-7381-9), 2005.
- Elith, J., Leathwick, J. R., and Hastie, T.: A working guide to boosted regression trees, *Journal of Animal Ecology*, 77, 802-813, <https://doi.org/10.1111/j.1365-2656.2008.01390.x>, 2008.
- Fan, J., Wang, X., Wu, L., Zhou, H., Zhang, F., Yu, X., Lu, X., and Xiang, Y.: Comparison of support vector machine and extreme gradient boosting for predicting daily global solar radiation using temperature and precipitation in humid subtropical climates: A case study in china, *Energy Conversion and Management*, 164, 102-111, <https://doi.org/10.1016/j.enconman.2018.02.087>, 2018.
- ~~Fawcett, T.: An introduction to roc analysis, *Pattern Recognition Letters*, 27, 861-874, <https://doi.org/10.1016/j.patrec.2005.10.010>, 2006.~~

- Filzmoser, P., Hron, K., and Reimann, C.: Univariate statistical analysis of environmental (compositional) data: Problems and possibilities, *Science of the Total Environment*, 407, 6100-6108, <https://doi.org/10.1016/j.scitotenv.2009.08.008>, 2009.
- 5 Follain, S., Minasny, B., McBratney, A. B., and Walter, C.: Simulation of soil thickness evolution in a complex agricultural landscape at fine spatial and temporal scales, *Geoderma*, 133, 71-86, <https://doi.org/10.1016/j.geoderma.2006.03.038>, 2006.
- Fu, G.-H., Xu, F., Zhang, B.-Y., and Yi, L.-Z.: Stable variable selection of class-imbalanced data with precision-recall criterion, *Chemometrics and Intelligent Laboratory Systems*, 171, 241-250, <https://doi.org/10.1016/j.chemolab.2017.10.015>, 2017.
- 10 Gobin, A., Campling, P., and Feyen, J.: Soil-landscape modelling to quantify spatial variability of soil texture, *Physics and Chemistry of the Earth Part B-Hydrology Oceans and Atmosphere*, 26, 41-45, [https://doi.org/10.1016/s1464-1909\(01\)85012-7](https://doi.org/10.1016/s1464-1909(01)85012-7), 2001.
- Gochis, D. J., Vivoni, E. R., and Watts, C. J.: The impact of soil depth on land surface energy and water fluxes in the north american monsoon region, *Journal of Arid Environments*, 74, 564-571, <https://doi.org/10.1016/j.jaridenv.2009.11.002>, 15 2010.
- Gower, J. C.: Algorithm as 78: The mediancentre. *Journal of the Royal Statistical Society. Series C (Applied Statistics)*, 23, 466-470. [10.2307/2347150](https://doi.org/10.2307/2347150), 1974.
- Grunsky, E. C.: The interpretation of geochemical survey data, *Geochemistry: Exploration, Environment, Analysis*, 10, 27, [10.1144/1467-7873/09-210](https://doi.org/10.1144/1467-7873/09-210), 2010.
- 20 Hengl, T., Heuvelink, G. B. M., Kempen, B., Leenaars, J. G. B., Walsh, M. G., Shepherd, K. D., Sila, A., MacMillan, R. A., de Jesus, J. M., Tamene, L., and Tondoh, J. E.: Mapping soil properties of africa at 250 m resolution: Random forests significantly improve current predictions, *Plos One*, 10, <https://doi.org/10.1371/journal.pone.0125814>, 2015.
- Hengl, T., de Jesus, J. M., Heuvelink, G. B. M., Gonzalez, M. R., Kilibarda, M., Blagotic, A., Shangguan, W., Wright, M. N., Geng, X., Bauer-Marschallinger, B., Guevara, M. A., Vargas, R., MacMillan, R. A., Batjes, N. H., Leenaars, J. G. B., 25 Ribeiro, E., Wheeler, I., Mantel, S., and Kempen, B.: Soilgrids250m: Global gridded soil information based on machine learning, *Plos One*, 12, <https://doi.org/10.1371/journal.pone.0169748>, 2017.
- Heung, B., Ho, H. C., Zhang, J., Knudby, A., Bulmer, C. E., and Schmidt, M. G.: An overview and comparison of machine-learning techniques for classification purposes in digital soil mapping, *Geoderma*, 265, 62-77, <https://doi.org/10.1016/j.geoderma.2015.11.014>, 2016.
- 30 Huang, J., Subasinghe, R., and Triantafyllis, J.: Mapping particle-size fractions as a composition using additive log-ratio transformation and ancillary data, *Soil Science Society of America Journal*, 78, 1967-1976, <https://doi.org/10.2136/sssaj2014.05.0215>, 2014.

- Huete, A., Didan, K., Miura, T., Rodriguez, E. P., Gao, X., and Ferreira, L. G.: Overview of the radiometric and biophysical performance of the modis vegetation indices, *Remote Sensing of Environment*, 83, 195-213, [https://doi.org/10.1016/s0034-4257\(02\)00096-2](https://doi.org/10.1016/s0034-4257(02)00096-2), 2002.
- Huete, A. R.: A soil-adjusted vegetation index (savi), *Remote Sensing of Environment*, 25, 295-309, [https://doi.org/10.1016/0034-4257\(88\)90106-x](https://doi.org/10.1016/0034-4257(88)90106-x), 1988.
- 5 Jafari, A., Khademi, H., Finke, P. A., Van de Wauw, J., and Ayoubi, S.: Spatial prediction of soil great groups by boosted regression trees using a limited point dataset in an arid region, southeastern iran, *Geoderma*, 232, 148-163, <https://doi.org/10.1016/j.geoderma.2014.04.029>, 2014.
- Krasilnikov, P. V., Garcia-Calderon, N. E., Ibanez-Huerta, A., Bazan-Mateos, M., and Hernandez-Santana, J. R.: Soilscales 10 in the dynamic tropical environments: The case of sierra madre del sur, *Geomorphology*, 135, 262-270, <https://doi.org/10.1016/j.geomorph.2011.02.013>, 2011.
- Kuhn, M.: Caret: Classification and regression training, R package version 6.0-80, available at: <https://CRAN.R-project.org/package=caret> (last access: 18 November 2018), 2018.
- Landis, J. R., and Koch, G. G.: Measurement of observer agreement for categorical data, *Biometrics*, 33, 159-174, <https://doi.org/10.2307/2529310>, 1977.
- 15 Lark, R. M., and Bishop, T. F. A.: Cokriging particle size fractions of the soil, *European Journal of Soil Science*, 58, 763-774, <https://doi.org/10.1111/j.1365-2389.2006.00866.x>, 2007.
- Liaw, A., and Wiener, M.: Classification and regression by randomforest, *R News*, 2, 18-22, 2002.
- Liess, M., Glaser, B., and Huwe, B.: Uncertainty in the spatial prediction of soil texture comparison of regression tree and 20 random forest models, *Geoderma*, 170, 70-79, <https://doi.org/10.1016/j.geoderma.2011.10.010>, 2012.
- Marchetti, A., Piccini, C., Santucci, S., Chiuchiarelli, I., and Francaviglia, R.: Simulation of soil types in teramo province (central italy) with terrain parameters and remote sensing data, *Catena*, 85, 267-273, <https://doi.org/10.1016/j.catena.2011.01.012>, 2011.
- Martin-Fernandez, J. A., Olea-Meneses, R. A., and Pawlowsky-Glahn, V.: Criteria to compare estimation methods of 25 regionalized compositions, *Mathematical Geology*, 33, 889-909, <https://doi.org/10.1023/a:1012293922142>, 2001.
- McBratney, A. B., Santos, M. L. M., and Minasny, B.: On digital soil mapping, *Geoderma*, 117, 3-52, [https://doi.org/10.1016/s0016-7061\(03\)00223-4](https://doi.org/10.1016/s0016-7061(03)00223-4), 2003.
- McNamara, J. P., Chandler, D., Seyfried, M., and Achet, S.: Soil moisture states, lateral flow, and streamflow generation in a semi-arid, snowmelt-driven catchment, *Hydrological Processes*, 19, 4023-4038, <https://doi.org/10.1002/hyp.5869>, 2005.
- 30 Menafoglio, A., Guadagnini, A., and Secchi, P.: A kriging approach based on aitchison geometry for the characterization of particle-size curves in heterogeneous aquifers, *Stoch. Environ. Res. Risk Assess.*, 28, 1835-1851, <https://doi.org/10.1007/s00477-014-0849-8>, 2014.
- Menafoglio, A., Guadagnini, A., and Secchi, P.: Stochastic simulation of soil particle-size curves in heterogeneous aquifer systems through a bayes space approach, *Water Resources Research*, 52, 5708-5726, 10.1002/2015wr018369, 2016a.

- Menafoglio, A., Secchi, P., and Guadagnini, A.: A class-kriging predictor for functional compositions with application to particle-size curves in heterogeneous aquifers, *Math Geosci.*, 48, 463-485, <https://doi.org/10.1007/s11004-015-9625-7>, 2016b.
- Metternicht, G. I., and Zinck, J. A.: Remote sensing of soil salinity: Potentials and constraints, *Remote Sensing of Environment*, 85, 1-20, [https://doi.org/10.1016/s0034-4257\(02\)00188-8](https://doi.org/10.1016/s0034-4257(02)00188-8), 2003.
- 5 Meyer, D., Dimitriadou, E., Hornik, K., Andreas, W., and Friedrich, L.: E1071: Misc functions of the department of statistics, probability theory group (formerly: E1071), tu wien, R package version 1.6-8, available at: <https://CRAN.R-project.org/package=e1071> (last access: 18 November 2018), 2017.
- Moeys, J.: Soiltexture: Functions for soil texture plot, classification and transformation, R package version 1.4.6, available at: <https://CRAN.R-project.org/package=soiltexture> (last access: 18 November 2018), 2018.
- 10 Odeh, I. O. A., Todd, A. J., and Triantafyllis, J.: Spatial prediction of soil particle-size fractions as compositional data, *Soil Science*, 168, 501-515, <https://doi.org/10.1097/00010694-200307000-00005>, 2003.
- Pahlavan-Rad, M. R., and Akbarimoghaddam, A.: Spatial variability of soil texture fractions and ph in a flood plain (case study from eastern iran), *Catena*, 160, 275-281, <https://doi.org/10.1016/j.catena.2017.10.002>, 2018.
- 15 Poggio, L., and Gimona, A.: 3d mapping of soil texture in scotland, *Geoderma Regional*, 9, 5-16, <https://doi.org/10.1016/j.geodrs.2016.11.003>, 2017.
- R Core Team: R: A language and environment for statistical computing, R Foundation for Statistical Computing, Vienna, Austria. available at: <https://www.R-project.org/> (last access: 18 November 2018), 2018.
- 2018.
- 20 Reimann, C., and Filzmoser, P.: Normal and lognormal data distribution in geochemistry: Death of a myth. Consequences for the statistical treatment of geochemical and environmental data, *Environmental Geology*, 39, 1001-1014, <https://doi.org/10.1007/s002549900081>, 2000
- Saito, T., and Rehmsmeier, M.: Precrec: Fast and accurate precision-recall and roc curve calculations in r, *Bioinformatics*, 33, 145-147, <https://doi.org/10.1093/bioinformatics/btw570>, 2017.
- 25 Salazar, E., Giraldo, R., and Porcu, E.: Spatial prediction for infinite-dimensional compositional data, *Stochastic Environmental Research and Risk Assessment*, 29, 1737-1749, <https://doi.org/10.1007/s00477-014-1010-4>, 2015.
- Schliep, K., and Hechenbichler, K.: Kknn: Weighted k-nearest neighbors, R package version 1.3.1, available at: <https://CRAN.R-project.org/package=kknn> (last access: 18 November 2018), 2016.
- Small, C. G.: A survey of multidimensional medians, *International Statistical Review*, 58, 263-277, 10.2307/1403809, 1990.
- 30 Song, X.-D., Brus, D. J., Liu, F., Li, D.-C., Zhao, Y.-G., Yang, J.-L., and Zhang, G.-L.: Mapping soil organic carbon content by geographically weighted regression: A case study in the heihe river basin, china, *Geoderma*, 261, 11-22, <https://doi.org/10.1016/j.geoderma.2015.06.024>, 2016.
- Streiner, D. L.: Maintaining standards: Differences between the standard deviation and standard error, and when to use each, *Canadian Journal of Psychiatry-Revue Canadienne De Psychiatrie*, 41, 498-502, 10.1177/070674379604100805, 1996.

- Subasi, A.: Eeg signal classification using wavelet feature extraction and a mixture of expert model, *Expert Systems with Applications*, 32, 1084-1093, <https://doi.org/10.1016/j.eswa.2006.02.005>, 2007.
- Sun, X.-L., Wu, Y.-J., Wang, H.-L., Zhao, Y.-G., and Zhang, G.-L.: Mapping soil particle size fractions using compositional kriging, cokriging and additive log-ratio cokriging in two case studies, *Mathematical Geosciences*, 46, 429-443, <https://doi.org/10.1007/s11004-013-9512-z>, 2014.
- 5 Taalab, K., Corstanje, R., Zawadzka, J., Mayr, T., Whelan, M. J., Hannam, J. A., and Creamer, R.: On the application of bayesian networks in digital soil mapping, *Geoderma*, 259, 134-148, <https://doi.org/10.1016/j.geoderma.2015.05.014>, 2015.
- Taghizadeh-Mehrzardi, R., Nabiollahi, K., Minasny, B., and Triantafilis, J.: Comparing data mining classifiers to predict spatial distribution of usda-family soil groups in baneh region, iran, *Geoderma*, 253, 67-77, <https://doi.org/10.1016/j.geoderma.2015.04.008>, 2015.
- 10 Thompson, J. A., Roecker, S., Grunwald, S., and Owens, P. R.: Chapter 21 - digital soil mapping: Interactions with and applications for hydropedology, in: *Hydropedology*, edited by: Lin, H., Academic Press, Boston, 665-709, 2012.
- van den Boogaart, K. G., and Tolosana-Delgado, R.: "Compositions": A unified r package to analyze compositional data, *Computers & Geosciences*, 34, 320-338, <https://doi.org/10.1016/j.cageo.2006.11.017>, 2008.
- 15 Vapnik, V.: The support vector method of function estimation, *Nonlinear modeling: Advanced black-box techniques*, edited by: Suykens, J. A. K., and Vandewalle, J., 55-85 pp., 1998.
- Walvoort, D. J. J., and de Gruijter, J. J.: Compositional kriging: A spatial interpolation method for compositional data, *Mathematical Geology*, 33, 951-966, <https://doi.org/10.1023/a:1012250107121>, 2001.
- 20 Wang, Z., and Shi, W.: Mapping soil particle-size fractions: A comparison of compositional kriging and log-ratio kriging, *Journal of Hydrology*, 546, 526-541, <https://doi.org/10.1016/j.jhydrol.2017.01.029>, 2017.
- Wang, Z., and Shi, W.: Robust variogram estimation combined with isometric log-ratio transformation for improved accuracy of soil particle-size fraction mapping, *Geoderma*, 324, 56-66, <https://doi.org/10.1016/j.geoderma.2018.03.007>, 2018.
- 25 Wu, B., Yan, N., Xiong, J., Bastiaanssen, W. G. M., Zhu, W., and Stein, A.: Validation of etwatch using field measurements at diverse landscapes: A case study in hai basin of china, *Journal of Hydrology*, 436, 67-80, <https://doi.org/10.1016/j.jhydrol.2012.02.043>, 2012.
- Wu, W., Li, A.-D., He, X.-H., Ma, R., Liu, H.-B., and Lv, J.-K.: A comparison of support vector machines, artificial neural network and classification tree for identifying soil texture classes in southwest china, *Computers and Electronics in Agriculture*, 144, 86-93, <https://doi.org/10.1016/j.compag.2017.11.037>, 2018.
- 30 Yang, R.-M., Zhang, G.-L., Liu, F., Lu, Y.-Y., Yang, F., Yang, F., Yang, M., Zhao, Y.-G., and Li, D.-C.: Comparison of boosted regression tree and random forest models for mapping topsoil organic carbon concentration in an alpine ecosystem, *Ecological Indicators*, 60, 870-878, <https://doi.org/10.1016/j.ecolind.2015.08.036>, 2016.

- Yi, C., Li, D., Zhang, G., Zhao, Y., Yang, J., Liu, F., and Song, X.: Criteria for partition of soil thickness and case studies, *Acta Pedologica Sinica*, 52, 220-227, 2015.
- Yoo, K., Amundson, R., Heimsath, A. M., and Dietrich, W. E.: Spatial patterns of soil organic carbon on hillslopes: Integrating geomorphic processes and the biological c cycle, *Geoderma*, 130, 47-65, <https://doi.org/10.1016/j.geoderma.2005.01.008>, 2006.
- 5 Zeraatpisheh, M., Ayoubi, S., Jafari, A., and Finke, P.: Comparing the efficiency of digital and conventional soil mapping to predict soil types in a semi-arid region in iran, *Geomorphology*, 285, 186-204, <https://doi.org/10.1016/j.geomorph.2017.02.015>, 2017.
- Zeraatpisheh, M., Ayoubi, S., Jafari, A., Tajik, S., and Finke, P.: Digital mapping of soil properties using multiple machine learning in a semi-arid region, central iran, *Geoderma*, <https://doi.org/10.1016/j.geoderma.2018.09.006>, 2018.
- 10 Zhang, S.-w., Shen, C.-y., Chen, X.-y., Ye, H.-c., Huang, Y.-f., and Lai, S.: Spatial interpolation of soil texture using compositional kriging and regression kriging with consideration of the characteristics of compositional data and environment variables, *Journal of Integrative Agriculture*, 12, 1673-1683, [https://doi.org/10.1016/s2095-3119\(13\)60395-0](https://doi.org/10.1016/s2095-3119(13)60395-0), 2013.
- 15 Zhao, Z., Chow, T. L., Rees, H. W., Yang, Q., Xing, Z., and Meng, F.-R.: Predict soil texture distributions using an artificial neural network model, *Computers and Electronics in Agriculture*, 65, 36-48, <https://doi.org/10.1016/j.compag.2008.07.008>, 2009.